Spatial variations of biochemical content and stable isotope ratios of size-fractionated plankton in the Mediterranean Sea (MERITE-HIPPOCAMPE campaign)

Tesán-Onrubia Javier Angel [1, *], Tedetti Marc [1], Carlotti François [1], Tenaille Melissa [1], Guilloux Loïc [1], Pagano Marc [1], Lebreton Benoit [2], Guillou Gaël [2], Fierro-González Pamela [1], Guigue Catherine [1], Chifflet Sandrine [1], Garcia Théo [1], Boudriga Ismail [3], Belhassen Malika [3], Zouari Amel Bellaaj [3], Bănaru Daniela [1, *]

[1] Aix Marseille Univ., Université de Toulon, CNRS, IRD, MIO UM 110, 13288 Marseille, France
[2] UMR 7266 Littoral Environnement et Sociétés (CNRS - La Rochelle Université), La Rochelle, France
[3] Institut National des Sciences et Technologies de la Mer (INSTM), 28, rue 2 mars 1934, 24, Salammbô 2025, Tunisia

* Corresponding authors : Javier Angel Tesan-Onrubia,
email address : javier.tesan@mio.osupytheas.fr ; Daniela Banaru, email address :
daniela.banaru@mio.osupytheas.fr

Abstract :

Plankton represents the main source of carbon in marine ecosystems and is consequently an important gateway for contaminants into the marine food webs. During the MERITE– HIPPOCAMPE campaign in the Mediterranean Sea (April–May 2019), plankton was sampled from pumping and net tows at 10 from the French coast to the Gulf of Gabès (Tunisia) to obtain different size fractions in contrasted regions. This study combines various approaches, including biochemical analyses, analyses of stable isotope ratios (δ13C, δ15N), cytometry analyses and mixing models (MixSiar) on size-fractions of phyto- and zooplankton from 0.7 to >2000 μm. Pico- and nanoplankton represented a large energetic resource at the base of pelagic food webs. Proteins, lipids, and stable isotope ratios increased with size in zooplankton and were higher than in phytoplankton. Stable isotope ratios suggest different sources of carbon and nutrients at the base of the planktonic food webs depending on the coast and the offshore area. In addition, a link between productivity and trophic pathways was shown, with high trophic levels and low zooplankton biomass recorded in the offshore area. The results of our study highlight spatial variations of the trophic structure within the plankton size-fractions and will contribute to assess the role of the plankton as a biological pump of contaminants.

Keywords : Phytoplankton, Zooplankton, 813C, 815N, Plankton trophic structure, Contaminants

1. Introduction

Phyto- and zooplankton play a central role in the functioning of marine ecosystems by producing, transforming and transferring the organic matter up to planktivorous species (Bănaru et al., 2019; Chen et al., 2022). Plankton thus represents the main source of carbon fueling the marine food webs (Bănaru et al., 2013; Cresson et al., 2020). Phyto- and zooplankton are composed of a myriad of organisms of great diversity in terms of size, metabolism, physiology, and diet that are governed by different trophic pathways, and complex ecological interactions. As taxonomic composition strongly differs between planktonic size-fractions, a size-based approach has become widely used to study the structure and functioning of the planktonic compartment (Rau et al., 1990; Rolff, 2000; Carlotti et al., 2008; Hunt et al., 2017). In pelagic food webs, body size determines rates of production (Banse and Mosher, 1980), energy requirements (Brown et al., 2004), mortality rates (Hirst and Kiørboe, 2002) and predator-prey interactions (Cohen et al., 1993; Ljungström et al., 2020). The biochemical composition of the different plankton size-fractions provides information on their energetic content, which may influence prey selection (Carlotti et al., 2008, Harmelin-Vivien et al., 2019; Chen et al., 2019, 2021, 2022), while the carbon and nitrogen isotopic ratios ($\delta^{13}C$ and $\delta^{15}N$ values) of the plankton size-fractions provide information on the fluxes of organic matter within the planktonic food webs (Peterson et al., 1985; Cabana and Rasmussen, 1994; Vander Zanden and Rasmussen, 2001).

Besides its central role in the functioning of marine ecosystems, plankton is now recognized as a key gateway of inorganic and organic contaminants into the marine food web (Tao et al., 2018; Chouvelon et al., 2019; Tedetti et al., 2023). Phytoplankton is exposed to contaminants *via* water. Bioconcentration of contaminants in phytoplankton is driven mainly by partition equilibrium processes between the cells and the surrounding water (Frouin et al., 2013). For a given species or cell size of phytoplankton, and a given physico-chemical habitat (temperature, organic carbon content, etc.), the bioconcentration factors of organic contaminants may be directly correlated with their octanol-water partitioning coefficients (log K_{ow}), i.e., their degree of lipophilicity/hydrophobicity (Frouin et al., 2013). Correspondingly, the bioconcentration of a given contaminant has been shown to increase with decreasing size of phytoplankton (Fan and Reinfelder, 2003). Bioaccumulation processes in zooplankton are highly complex due to the entry of contaminants by both the water aqueous phase (bioconcentration) and diet, the trophic interactions and/or transfers between phytoplankton and various zooplankton, and the contaminant removal processes used by these organisms

78   (Tiano et al., 2014; Alekseenko et al., 2018; Tao et al., 2018). Biomagnification may also

79   occur between the low and high trophic level organisms in the marine food webs (Chouvelon

80   et al., 2019).

81   Therefore, the uptake, accumulation, and transfer of contaminants within the planktonic food

82   webs may be strongly influenced by its characteristics such as the size-fraction distribution,

83   the biochemical/energetic content (Hennig, 1986; Mason et al., 1995; Wu and Wang, 2011),

84   the trophic interactions and the fluxes of organic matter (Peterson et al., 1985; Cabana and

85   Rasmussen, 1994; Vander Zanden and Rasmussen, 2001). Characterizing the content of

86   phyto-, and zooplankton in terms of size-fraction, biochemical/energetic content and stable

87   isotope ratios (δ^{13}C and δ^{15}N) may thus provide key information on the structure, functioning,

88   and trophic interactions of this planktonic food webs, but also on the capacity of accumulation

89   and transfer of organic and inorganic contaminants within this planktonic network and

90   potentially their transfer to higher trophic levels.

91   The Mediterranean Sea has a high diversity of planktonic and exploited resources, and

92   contrasted biogeographical regions impacted by climate change and human activities (Durrieu

93   de Madron et al., 2011; Mayot et al., 2017). As the Mediterranean Sea is mainly oligotrophic,

94   its autotrophic biomass is dominated by small-size pico- and nanophytoplankton groups

95   (Leblanc et al., 2018; Boudriga et al., 2022). These groups play a key role in the biomass and

96   energy transfer to zooplankton (Bănaru et al., 2014; Hunt et al., 2017; Leblanc et al., 2018).

97   However, coastal areas impacted by riverine and urban inputs may locally be more enriched

98   and sometimes can even be characterized by higher phytoplankton biomass dominated by

99   larger cells such as dinobionts and diatoms (Harmelin-Vivien et al., 2008). Champalbert

100   (1996) highlighted spatial differences in the zooplankton diversity and biomass, with a lower

101   diversity and a higher biomass in coastal waters relative to offshore areas. The Mediterranean

102   Sea is also strongly exposed to chemical contamination due to the intensive human activities

103   in the bordering countries, its semi-closed status that limits the dilution of contaminants, and

104   the relatively short ventilation and residence times its waters (Durrieu de Madron et al., 2011;

105   Tedetti et al., 2023).

106   In this context, the aims of this work, carried out in the frame of the MERITE-HIPPOCAMPE

107   campaign, were: 1) to investigate the structure and functioning (in terms of trophic

108   interactions and organic matter fluxes) of the planktonic food webs of the Mediterranean Sea

109   through the characterization of the biomass, biochemical/energetic content and δ^{13}C/δ^{15}N

110   ratios of several size-fractions of phyto- and zooplankton ranging from 0.7 to > 2000 µm, 2)

111   to explore variations in size-spectra and spatial variations of these characteristics

4

112 (biochemical/energetic content and $\delta^{13}C/\delta^{15}N$ ratios), and relate these variations to their

113 composition (*via* cytometry and imagery analyses) and also to the specificities of the studied

114 areas, and 3) to discuss the implications of these findings regarding the accumulation and

115 transfer of contaminants in the planktonic food webs.

116 To our knowledge, this work represents the first study to use a wide variety of approaches,

117 and methodologies, such as biochemical analyses (proteins, carbohydrates, lipids and energy),

118 analyses of isotopic ratios ($\delta^{13}C$, $\delta^{15}N$), cytometry analyses and mixing models (MixSiar) on

119 fine size-fractions of phyto- and zooplankton ranging from 0.7 to > 2000 µm for the purpose

120 of studying plankton food webs. The use of innovative sampling techniques, such as the

121 deployment of *in situ* pumps equipped with a sequential filtration system, or the towing of a

122 MultiNet device in chlorophyll maximum layer (CML), enabled us to obtain large amounts of

123 size fractionated phyto- and zooplankton, material rarely acquired together.

124

125   **2.   Material and methods**

126

127   **2.1. Study area and sampling**

128 The MERITE-HIPPOCAMPE cruise was conducted in the Mediterranean Sea in spring 2019,

129 from April 13 to May 14, onboard the R/V *Antea* (Tedetti and Tronczynski, 2019; Tedetti et

130 al., 2023). Ten stations were sampled from the French coast (La Seyne-sur-Mer, Northwestern

131 Mediterranean) to the Gulf of Gabès in Tunisia (Southeastern Mediterranean) in coastal and

132 offshore locations, including the Gulf of Lion, the Ligurian and Algerian consensus regions,

133 the North Balearic Front and Sicilian Channel areas, and the gulfs of Hammamet and Gabès,

134 which presented different hydrological, biogeochemical and bloom conditions, and different

135 levels of anthropogenic pressures (Fig. 1, Table S1). Phytoplankton and zooplankton were

136 sampled at each station at the CML, during spring bloom (April to May), when maximum

137 primary and secondary production occurs (Liénart et al., 2018; Tedetti et al., 2023).

138 Suspended particulate matter (SPM) was collected and filtered using McLane Large Volume

139 Water Transfer System Samplers (WTS6-142LV, 4–8 L min^{-1}), hereinafter referred to as

140 McLane *in situ* pumps. One pump was mounted with a regular 142-mm filter-holder holding

141 one 142-mm-diameter filter. This pump was equipped with a ~ 0.7-µm-pore-size pre-

142 combusted pre-weighed GF/F filter (Whatman) and covered with a 60-µm-pore-size

143 homemade sock-type pre-filter so that the filtered particle size-fraction was 0.7–60 µm. A

144 second McLane *in situ* pump was mounted with a mini-Multiple Unit Large Volume *in situ*

145 Filtration System (MULVFS) filter holder composed of baffle tubes on the top followed by

146 successive baffle and filter support plates, for sequential filtration with three different filters

147 (142-mm diameter) (Bishop et al., 2012). The filter series used were one ~ 0.7-µm-pore-size

148 pre-combusted (450 °C, 6 h), pre-weighed GF/F filter, one 2.7-µm-pore-size pre-combusted,

149 pre-weighed GF/D filter (Whatman), and one 20-µm-pore-size pre-cleaned (HCl 0.05% v/v)

150 pre-weighed home-made Nylon filter so that the filtered particle size fractions were 0.7–2.7,

151 2.7–20, and > 20 µm (hereafter labeled 20–60 µm). The pumps were deployed in the CML

152 between 40 and 60 min. The volumes of filtered seawater ranged between 169 and 300 L

153 depending on the stations. After pump deployment, filters were 'dried' by connecting the filter

154 holder to a vacuum pump, stored in pre-combusted (450 °C, 6 h) aluminum sheets, and

155 conserved at –20 °C and then freeze-dried. Then, punches with a known surface area were

156 made into filters to obtain subsamples for the different analyses.

157 Zooplankton was sampled using a Multinet Plankton Sampler (Midi type with 0.25-m^2

158 aperture, Hydro-Bios), referred to hereafter as 'MultiNet', towed horizontally in the CML. The

159 MultiNet position was maintained stable at the defined layer by means of a V-fin deflector

160 and controlled vessel speed (2.5 knots), and real-time control of its position from the onboard

161 desk-unit. The MultiNet was mounted with five individual (exchangeable) 2.5-m-long nylon

162 nets with a mesh size of 60-µm and cod ends of the same mesh size. The MultiNet frame was

163 equipped with various sensors: two Hydro-Bios flowmeters (one at the mouth and the other

164 on the side) to assess the volume of water filtered by the nets, a CTD sensor and a total

165 chlorophyll *a* (TChl*a*) fluorometer. Connected to the onboard desk unit *via* the electro-

166 mechanical cable, these captors inform on *in situ* depth, TChl*a* concentration, filtered volume

167 and flow rate, allowing the operator to decide to open and close the nets. Nets were closed

168 when the flow rate reached a threshold value to limit clogging. Filtered volumes for each net

169 reached up to 185 m^3. Once the five nets were filled, the MultiNet was hauled back on board,

170 and the five cod ends linked by a helicoidal bucket connector were carefully recovered. The

171 fifth net remained open until the end of the operation, filtering the layer between the CML

172 and the surface. The cod ends were rinsed out with local seawater, and their content

173 transferred to pre-cleaned 10-L PFA bottles. The MultiNet was then returned to the water.

174 This operation was repeated several times to get sufficient amounts of plankton for all

175 possible further contaminant content analyses (Tedetti et al., 2023). In the clean onboard

176 container lab, plankton collected in PFA bottles was then size-fractionated through a column

177 of five stainless steel sieves (60, 200, 500, 1000 and 2000 µm mesh-size) by wet-sieving with

178 seawater previously filtered onto GF/F filters and stored in stainless steel jerrycans to obtain

179 the following size-fractions: 60–200, 200–500, 500–1000, 1000–2000 and > 2000 µm.

180   Samples were stored in pre-combusted (450 °C, 6 h) Pyrex bottles, conserved at –20 °C and

181   freeze-dried. Large fractions (> 2000 µm) were most likely under-sampled compared to

182   smaller fractions. These fractions should be carefully treated because they represent a

183   relatively low – and difficult to estimate – biomass, form colonies, and may actively evade

184   capture by swimming. The detailed methods to determine zooplankton group composition

185   analysis presented in this paper and related to our results are detailed in Fierro-González et al.

186   (2023).

187

188   **2.2. Analyses**

189

190   **2.2.1. Particulate organic carbon and nitrogen**

191   Samples (i.e., 22-mm diameter filter or 1 mg dry weight DW zooplankton) were leached with

192   100 µL of sulfuric acid (H_2SO_4 0.5 mol L^{-1}) to remove any inorganic carbon. Samples were

193   then stored in 25 mL Schott® glass bottles for subsequent analyses. Filter blanks were

194   conditioned with 1 mL of ethanol and with 600 mL of 0.2-µm filtered seawater.

195   Determination of particulate organic carbon (POC) and nitrogen (PON) concentrations were

196   carried out simultaneously on the same sample using the persulfate wet-oxidation procedure

197   according to Raimbault et al. (1999).

198

199   **2.2.2. Suspended particulate matter and plankton dry weight**

200   Suspended particulate matter dry weight (SPM_{DW}) was measured in the 0.7–60 and 20–60-µm

201   filters gravimetrically by weighing the tare, wet and dry filters with a precision balance (d =

202   0.01 mg). Briefly, we subtracted from the dry filter the tare and the salts associated with the

203   evaporated water, considering a salinity of 38. Tests conducted with filtered seawater

204   evidenced a higher mass after drying than the salt present in water, and most likely related to

205   the highly hygroscopic characteristics of salts. A ratio of 1.2 between the observed mass and

206   the theoretical mass associated with salt was applied to correct the water bonded to salt. When

207   biomasses were low, as for 0.7–2.7 and 2.7–20-µm filters, high uncertainty in weighing

208   increased the margin of error. SPM_{DW} in the 0.7–2.7 and 2.7–20-µm filters were thus

209   estimated by multiplying their relative fraction of POC by the biomass measured

210   gravimetrically in the 0.7–60-µm size-fraction. POC can be employed as a proxy of SPM_{DW},

211   based on the correlations assessed by Trimble and Baskaran (2005). SPM_{DW} at the CML is

212   mainly composed of POC (around 50%) but also contains biogenic silica, calcium carbonate

213   and lithogenic matter (Bishop et al., 1977; Krasakopoulou and Karageorgis, 2005). On the

7

214 basis of these observations, relative POC was used to assess the contribution of the different

215 size-fractions to the total biomass. Plankton dry weight (Plankton $_{DW}$) of size fractions 60–

216 200, 200–500, 500–1000, 1000–2000, and > 2000 µm were determined after drying samples

217 on pre-weighed GF/F filters (60 °C, 24 h) and then re-weighed with a microbalance, taking

218 into consideration the volumes of water filtered by the MultiNet (Fierro-González et al.,

219 2023).

220

221   **2.2.3. Biochemical and energy content**

222 Biochemical compounds (proteins, carbohydrates, and lipids) were extracted in triplicate from

223 freeze-dried filters and zooplankton samples and expressed in µg mg^{-1} DW. Absorbance of

224 the extracts was then measured at different wavelengths using a spectrophotometer

225 (Shimadzu, UV-1280). Briefly, proteins were extracted using a Folin phenol reagent

226 following the Lowry et al. (1951) method and measured at 700 nm. Carbohydrates were

227 extracted using the phenol-sulfuric acid reaction described in Dubois et al. (1956) and

228 measured at 490 nm. Finally, lipids were extracted with a monophasic methanol-

229 dichloromethane solution (Bligh and Dyer, 1959) and measured at 360 nm. Ashes and

230 residual organic compounds not recovered by these standard biochemical assays (chitin for

231 example) may be estimated by subtracting the weight of the biochemical compounds from the

232 total dry weight, but were not presented in this study. The energy content (E_i) was estimated

233 by summing the three biochemical compounds after converting them into energetic units

234 (21.4 kJ g^{-1} for proteins, 17.2 kJ g^{-1} for carbohydrates and 35.6 kJ g^{-1} for lipids) (Postel et al.,

235 2000). The plankton energy amount (E_T) provided by plankton per cubic meter per station at

236 CML (kJ m^{-3}) was calculated for all the plankton size-fractions by multiplying the SPM$_{DW}$ or

237 the biomass (B_i in mg DW m^{-3}) of each size-fraction at a given station by its energy content

238 (E_i in kJ mg^{-1} DW) and the sum of E_T of all size-fractions represents the plankton total energy

239 amount, E_{TS}: $E_T = B_i \times E_i$.

240

241   **2.2.4. Stable isotope analyses (δ^{13}C and δ^{15}N)**

242 The SPM$_{DW}$ collected on filters was scraped off with a scalpel. Zooplankton samples were

243 ground to a fine powder with an agate mortar and pestle. Presence of carbonates on samples

244 can bias the measurement of δ^{13}C values as they are enriched in ^{13}C compared to organic

245 matter (Pinnegar and Polunin, 1999). Therefore, samples were acidified prior to the

246 measurement of δ^{13}C values of the particulate organic matter (POM). Samples were acidified

247 using HCl 1% and immediately rinsed with MilliQ-water. Measurements of δ^{15}N values of the

248   POM were carried out on raw samples. For zooplankton, approximately 0.5 mg of powder

249   was weighed into a tin cup (8 × 5 mm) using a precision balance (d = 0.01 mg). Carbon and

250   nitrogen stable isotope analyses were performed using a continuous-flow isotope-ratio mass

251   spectrometer (Delta V Plus, Thermo Scientific) with a Conflo IV interface coupled to an

252   elemental analyzer (EA Isolink, Thermo Scientific). Analyses were conducted at the Littoral,

253   Environment and Societies Joint Research Unit stable isotope facility (CNRS - University of

254   La Rochelle, France). The δ^{13}C and δ^{15}N values are expressed in δ notation as deviations from

255   standards (Vienna Pee Dee Belemnite for δ^{13}C and N_2 in air for δ^{15}N), in ‰, according to the

256   formula:

$$\delta X_{sample} = \left[\left(\frac{R_{sample}}{R_{standard}} \right) - 1 \right] \times 1000$$

257

258   where X is ^{13}C or ^{15}N, R_{sample} is the isotopic ratio of the sample and $R_{standard}$ is the isotopic ratio

259   of the standard. Calibration was carried out using reference materials (USGS-61, -62, -63 for

260   both carbon and nitrogen). The analytical precision of the measurements was < 0.10‰ for

261   carbon and nitrogen based on analyses of USGS-61 and USGS-63 used as laboratory internal

262   standards.

263

264   **2.2.5. Cytometry and imagery analyses**

265   For flow cytometry analyses, seawater was sampled with Niskin and Go-Flo bottles at the

266   CML. Seawater was filtered through a silk mesh filter with 100-µm pore size and then

267   immediately fixed with a 2% paraformaldehyde solution. Samples were incubated for 15 min

268   at 4 °C in the dark and then stored in liquid nitrogen onboard and at –80 °C in the laboratory

269   until analysis. The autotrophic pico- and nanoplankton were analyzed using a CyFlow®Space

270   flow cytometer (SysmexPartec) equipped with a blue diode pumped solid-state laser (20 mW;

271   488 nm) and a red diode laser (25 mW; 638 nm). Seawater samples were thawed in the dark,

272   filtered through a nylon mesh filter with a porosity of 30 µm (CellTrics®, SysmexPartec), and

273   mixed with flow check high-intensity beads of 2-µm diameter (Polysciences, USA). Cells

274   were characterized based on their scatter and fluorescence signals (Khammari et al., 2018)

275   and data were analyzed with the FloMax software (Sysmex Partec), which directly calculates

276   the cell concentration (cells cm^{-3}) of the resolved cell groups. Carbon biomass of each cell

277   group was estimated according to Khammari et al., (2020). The contributions of zooplankton,

278   phytoplankton (microalgae), and detritus components to the total Plankton DW were estimated

279   using imagery methods (FlowCAM and ZOOSCAN) according to Fierro-González et al.

280   (2023).

281

282   **2.3. Bayesian mixing model**

283   The contributions of the different size-fractions of phytoplankton (0.7–2.7, 2.7–20 and 20–60

284   µm) as food resources to zooplankton size-fractions and their confidence intervals were

285   estimated using a Bayesian mixing model using the R package MIXSIAR (Parnell et al.,

286   2013; https://github.com/brianstock/MixSIAR). This modeling approach incorporates

287   variability of potential food source isotopic compositions for consumers and of trophic

288   fractionation factors (TFF) and generates probability distributions of food source

289   contributions. The consumers (i.e., zooplankton) were grouped in the 60–500, 500–2000, and

290   > 2000-µm size-fractions based on statistical differences in their isotopic compositions.

291   Zooplankton size-fractions with similar isotopic compositions were thus considered to

292   consume the same food resources. Contributions were computed using δ^{13}C and δ^{15}N values.

293   As there is no well-established set of TFFs for plankton, we computed mixing model

294   estimates using the mean TFF values of 1.70 ± 0.38 ‰ for δ^{13}C and 2.40 ± 0.26 ‰ for δ^{15}N

295   (mean ± standard error (SE)), as established by Tiselius and Fransson (2016).

296

297   **2.4. Trophic level**

298   The trophic level (TL) of consumers was calculated following the equation proposed by Post

299   (2002):

$$\text{TL} = \left(\frac{\delta^{15}N_{consumer} - \delta^{15}N_{baseline}}{\text{TFF } \delta^{15}N} \right) + 1$$

300

301   where $\delta^{15}N_{consumer}$ is the isotopic composition of the consumer, $\delta^{15}N_{baseline}$ is the isotopic

302   composition of the size-fraction 0.7–2.7 µm considered as baseline with a trophic level of 1

303   and TFF δ^{15}N was fixed to 2.40 ± 0.26 ‰ (Tiselius and Fransson, 2016). TL of each size

304   fraction was weighted to its respective biomass per station (TL_B):

$$\text{TL}_B = \frac{\sum_i^n (\text{TL}_i * \% \text{ Biomass}_i)}{100}$$

305

306   where *I* is represented by each size fraction from 60–200 to > 2000 µm and n is the number of

307   size-fractions.

308

2.5. Data treatment

The effect of size-fractions and geographical area on the SPM_{DW}, $Plankton_{DW}$, POC, PON, C/N, carbon biomass of phytoplankton, biochemical composition, energy content, isotopic composition and trophic levels were tested by means of one-way ANOVA or non-parametric Kruskal-Wallis tests after testing for normality and homogeneity of variances, followed by appropriate paired comparison tests, using the software Statistica 12. Spearman's rank order correlation tests were used to assess the significance of the correlations between our results and some environmental variables (Tedetti et al., 2023).

3. Results

3.1. Plankton dry weight, TChl$a$, POC, PON and C:N

Significant differences in SPM_{DW} were observed between the different size-fractions (H = 23.2, p < 0.0001) (Table 1). When considering all stations, the highest mean SPM_{DW} was measured in the 2.7–20 µm size-fraction (0.18 ± 0.04 mg DW L^{-1}, n = 10) and the lowest in the 20–60 µm fraction (0.04 ± 0.02 mg DW L^{-1}, n = 10). Generally, these concentrations decreased from coastal stations to offshore stations, except for St9, which exhibited the highest SPM_{DW} in the 2.7–20 µm size-fraction (Table 1). The size-fractions 0.7–2.7 and 2.7–20 µm presented the lowest values at St15. The highest SPM_{DW} in the 20–60-µm size-fraction were observed at St17, St19 and St4. TChl$a$ concentrations in the > 0.7-µm fraction ranged from 0.21 (St17) to 1.54 µg L^{-1} (St9) with a mean value of 0.76 ± 0.14 µg L^{-1} (n = 10) (Table 1). The 60–200 and 200–500 µm zooplankton size-fractions showed the highest $Plankton_{DW}$ (Table 1). POC and PON concentrations increased with phytoplankton size with the lowest values in the 0.7–2.7 µm size-fraction (11.4 and respectively 2.1 µg C L^{-1}) and the highest ones in the 0.7–60 µm size-fraction (42.8 and respectively 6.9 µg C L^{-1}) (Table S2). The lowest POC and PON values were observed at St11 for the 0.7–2.7 µm size-fraction and at St2 for the 2.7–20 µm size-fraction (Table S2). The C:N ratios in the 0.7 to 60 µm size-fractions ranged from 5.7 at St19 to 8.5 at St9. The 0.7–2.7 µm size-fraction presented significantly lower C:N ratios than the 2.7–20-µm and the 20–60 µm size-fractions (Table S2).

3.2. Planktonic group composition

342 Different plankton groups contributed to the biomass of the different size-fractions. The size-
343 fraction 0.7–2.7 µm was on average dominated in biomass by *Synechococcus* spp. (4.6 µg C
344 L^{-1} or ~ 52%) and picoeukaryotes (4.0 µg C L^{-1} or ~ 45%) (Table S3). The size-fraction 2.7–
345 20 µm was dominated in biomass by the nanoeukaryotes (20.0 µg C L^{-1} ~ 88%) and
346 represented the highest biomass among size-fractions. The highest cumulated biomass in the
347 range 0.7–20 µm was found at St1, St9 and St19 (Table S3). POC concentration and the
348 carbon biomass of phytoplankton size-fractions between 0.7 and 20 µm showed a significant
349 linear correlation ($R^2 = 0.66$; p = 0.018) (Fig. S1). Carbon biomass estimated by flow
350 cytometry represented around 86% of the POC measured on filters (y = 0.86x + 11.86). Total
351 biomass was dominated by detritus and phytoplankton in the 60–200 and 200–500 µm size-
352 fractions (68.8 and 59.2%, respectively), which decreased with the increasing size-fractions
353 (10.5% in the > 2000-µm size-fraction) (Table S4). Copepods dominated in the zooplankton
354 biomass in the 60 to 2000 µm size-fractions (between 54.3% and 91.9%) while crustaceans
355 and gelatinous dominated the > 2000 µm size-fraction (Table S4).
356

357 3.3. Biochemical and energy content

358 The Mediterranean plankton sampled had for all size-fractions and stations combined, except
359 the 0.7–60-µm fraction, mean dry weight concentrations (± SE) of 222.6 ± 6.9 µg mg^{-1} DW (n
360 = 204) for proteins, 96.9 ± 6.5 µg mg^{-1} DW (n = 203) for carbohydrates, 35.1 ± 1.5 µg mg^{-1}
361 DW (n = 197) for lipids and an E$_i$ of 7.7 ± 0.2 kJ g^{-1} DW (n = 196).
362

363 3.3.1. Differences between plankton size-fractions

364 Considering all stations combined, the mean concentration of proteins increased with size and
365 was significantly higher in large fractions of zooplankton (500–1000 and 1000–2000 µm)
366 than in small fractions of phytoplankton (0.7–2.7 and 2.7–20 µm). The highest mean protein
367 concentration was recorded in the 1000–2000 µm size-fraction and the lowest in the largest (>
368 2000 µm) size-fraction (Fig. 2A). The mean concentration in carbohydrates decreased with
369 size. The concentrations measured in phytoplankton (0.7–60 and 20–60 µm) were
370 significantly higher than those of the large zooplankton (1000–2000 and > 2000 µm) (Fig.
371 2B). The mean concentration in lipids was quite homogeneous between size-fractions, with
372 the highest values measured in the size-fractions 20–60 and 1000–2000 µm, and lowest in the
373 size-fractions 0.7–2.7 and > 2000 µm (Fig. 2C). Energy content showed an increasing trend
374 with size for both phyto- and zooplankton size-fractions. The highest values were measured in

375 the 20–60 μm and 1000-2000 μm size-fractions, respectively, and the lowest in the size-

376 fractions 0.7–2.7 and > 2000 μm. (Fig. 2D).

377

378 ### 3.3.2. Differences between stations

379 To investigate the differences between stations, the size-fractions were grouped in two

380 fractions: the phytoplankton fraction (fractions between 0.7 and 60 μm) and the zooplankton

381 fraction (fractions between 60 and 500 μm that were sampled at all the stations). The highest

382 mean protein concentrations in phyto- and zooplankton fractions were recorded at St9, St11

383 and St15, and the lowest at St17 (Fig. 3A, B). The highest mean carbohydrate concentrations

384 were observed at St9 for the phytoplankton (Fig. 3C). The highest mean lipid concentrations

385 and energy values for phyto- and zooplankton were measured at St1, St2, St9 and St11, and

386 the lowest at St3, St4 and St17 (Fig. 3E-H). Overall, greater differences appeared between

387 stations than between size-fractions for most of these biochemical compounds (Table S5).

388 E_{TS} ranged from 1.17 kJ m^{-3} at St3 to 6.30 kJ m^{-3} at St9 with a mean value (± SE) of 2.37 ±

389 0.49 kJ m^{-3} (n = 10) (Fig. 4). High E_{TS} were also observed at coastal stations St1, St4, St17

390 and St19. The 0.7–2.7 and 2.7–20 μm size-fractions represented the largest energetic

391 reservoirs with mean values of 0.65 ± 0.09 kJ m^{-3} (n = 10) and 1.16 ± 0.37 kJ m^{-3} (n = 10),

392 respectively (Fig. 4). The 200–500-μm fraction represented the largest energy reservoir for

393 the zooplankton with a mean of 0.164 kJ m^{-3}. Although the 0.7–2.7 and 2.7–20 μm fractions

394 had lower E_i (6.2 and 6.3 kJ g^{-1} DW, respectively) than those measured in the > 60 μm size-

395 fractions (between 7.0 and 9.5 kJ g^{-1} DW) (Fig. 2), their dry weight was about one order of

396 magnitude higher (Tables 1 and S2), thus enhancing their major contribution of

397 phytoplankton to the total plankton energy amount available in the system (Fig. 4).

398

399 ## 3.4. Stable isotope compositions (δ^{13}C and δ^{15}N)

400 For all size fractions and stations combined, except the 0.7–60 μm fraction, the plankton δ^{13}C

401 values ranged from –26.6 to –17.4 ‰, with a mean of –23.0 ± 0.1‰ (n = 136), whereas the

402 δ^{15}N values ranged from –0.6 to 5.7‰, with a mean of 2.6 ± 0.1‰ (n = 136).

403

404 ### 3.4.1. Differences between plankton size-fractions

405 Considering all stations combined, the mean δ^{13}C and δ^{15}N values increased with size,

406 especially in the fractions ranging from 0.7 to 60 μm (Fig. 5, Table S6). Significantly higher

407 mean δ^{13}C values were reported in the 20–60 μm fraction than in the 0.7–2.7 μm fraction. The

408 mean δ^{15}N values of the size-fractions from 0.7 to 60 μm were all significantly different. Size-

409 fractions between 60 and 2000 µm showed slightly higher $\delta^{13}C$ values than those of smaller

410 fractions. The highest mean $\delta^{13}C$ and $\delta^{15}N$ values were measured in the 1000 to > 2000 µm

411 size-fractions (Fig. 5, Table S6).

412

413 **3.4.2. Differences between stations**

414 As for the biochemical composition, the size-fractions were grouped into two fractions: the

415 phytoplankton fraction (fractions between 0.7 and 60 µm) and the zooplankton fraction

416 (fractions between 60 and 500 µm that were sampled at all the stations). The mean $\delta^{13}C$ and

417 $\delta^{15}N$ values followed the same spatial variations between phyto- and zooplankton fractions

418 (Fig. 6A-D). For both phyto- and zooplankton, the highest mean $\delta^{13}C$ values were measured

419 at St4 and St17. The highest mean $\delta^{15}N$ values were detected in phytoplankton at St4, while

420 the lowest ones were observed at St9. In zooplankton, the highest mean $\delta^{15}N$ values were

421 measured at St10, and the lowest ones at St9, St17, and St19 (Fig. 6A-D). Overall, in contrast

422 to the biochemical composition, greater differences were highlighted between size-fractions

423 than between stations for both $\delta^{13}C$ and $\delta^{15}N$ values (Table S5).

424

425 **3.5. Trophic levels**

426 For all zooplankton size-fractions (60 to > 2000 µm) and stations combined, the TL ranged

427 from 1.5 to 3.6 with a mean of 2.2 ± 0.1 (n = 76). When considering all stations combined,

428 mean TL significatively increased with size (F = 5.2, p = 0.001) (Fig. 7). The highest mean

429 TL (2.6 ± 0.2, n = 10) was measured for the 1000–2000 µm size-fraction and the lowest TL

430 (1.9 ± 0.1, n = 20) in the 60–200 µm fraction. For the 60–200, 200–500, and 500–1000 µm

431 size-fractions, differences in mean TLs were overall significant between stations (H = 18.7, p

432 = 0.027; H = 18.9, p = 0.026 and H = 16.3, p = 0.037, respectively) with the highest mean

433 trophic levels by size-fraction at St10. Mean TL weighted by the plankton biomass (TL_B) had

434 values larger than 2 at St2, St3 in northern coastal waters, and at St9, St10 and St11 in

435 offshore waters (Fig. 8). The cumulated biomass of the zooplankton groups (60 to > 2000 µm)

436 of the sampled stations was significantly and negatively correlated with TL_B (R^2 = 0.61, p =

437 0.020) (Fig. S2).

438

439 **3.6. Trophic flows in the plankton food web**

440 The Mediterranean plankton food web analysis highlighted size predation (Fig. 9, Fig. S3).

441 For all stations combined, the 0.7–2.7 µm fraction was mainly consumed by the 60–500-µm

442 fraction, while the consumption of the 2.7–20 µm fraction was similar between the 60–500

443   and 500–2000-µm fractions. The > 2000 µm size-fraction mainly consumed the 20–60 µm

444   size fraction (Fig. 9, Fig. S3).

445

446   **4.   Discussion**

447

448   **4.1. Plankton biochemical content**

449   The present description of the plankton biochemical content along a north-south transect in

450   the Mediterranean Sea appears to be unique to our knowledge. The biochemistry of phyto-

451   and zooplankton has been extensively documented in many marine environments but remains

452   little observed in the Mediterranean Sea (Morris and Hopkins, 1983; Danovaro et al., 2000;

453   Yilmaz and Besiktepe, 2010; Chen et al., 2019).

454   Jónasdóttir (2019) summarizes the biochemistry of phytoplankton by a protein / carbohydrate

455   / lipid average ratio of 5 / 3 / 2 (with a range of 40–60, 17–40, and 16–26%), similar to Ríos et

456   al. (1998) who found a ratio of 4.9 / 3.2 / 1.9. In our study, the mean ratio of the size-fractions

457   between 0.7 and 60 µm was on average 5.6 / 3.6 / 0.9, therefore with relatively higher proteins

458   and lower lipids compared to previous ratios. The biochemical ratio in the > 60 µm size-

459   fractions was 6.9 / 2.0 / 1.1, reflecting higher protein and lower carbohydrate contents

460   compared to phytoplankton. The higher proportion of protein to carbohydrate is a good

461   indicator of the nitrogen availability in the environment whereas the inverse pattern may

462   reflect nitrogen-limited environments for both phyto- (Fabiano et al., 1999; Danovaro et al.,

463   2000; Yilmaz and Besiktepe, 2010; Kim et al., 2019) and zooplankton (Bhat et al., 1993).

464   Chen et al. (2019) found in spring time in the Bay of Marseille (in the same location as our

465   station St4), for the size-fraction 200–500 µm, carbohydrate concentrations (62.4 to 66.7 mg

466   g^{-1}) similar to ours, while their concentrations in lipids (98.3 to 102.8 mg g^{-1}) and proteins

467   (292.7 to 335.7 mg g^{-1}) were higher.

468   The protein and lipid concentrations were higher in zooplankton than in phytoplankton.

469   Within the zooplankton, an increase in proteins with size was observed, in agreement with

470   Guisande (2006). Most of the organisms in our samples between 60 and 2000 µm were

471   composed of copepods, and, consequently, the different fractions corresponding to different

472   life-stages of the same group (Fierro-González et al., 2023) may explain the size influence on

473   their biochemical content. The highest concentrations of carbohydrates and lipids reported in

474   the 20–60 µm size-fraction can be related to a mixed composition of microphyto- and

475   microzooplanktonic organisms, such as diatoms and metazoan eggs (Danovaro et al., 2000;

476   Chen et al., 2019). However, an underestimation of the SPM$_{DW}$ in the 20–60 µm fraction with

477   respect to that in the size-fractions from 0.7 to 60 µm – due to different estimation methods

478   (see section 2.2.2) – may explain the higher biochemical concentrations measured in the 20–

479   60 µm fractions. Finally, the lowest protein, carbohydrate, and lipid concentrations observed

480   in the > 2000-µm fraction were probably related to the dominance in this fraction of filter

481   feeder organisms, such as salps and siphonophores (Bănaru et al., 2014; Hunt et al., 2017;

482   Chen et al., 2019; Fierro-González et al., 2023).

    Organic contaminants have been shown to have a strong chemical affinity for lipids or

483   proteins (Mason et al., 1995; Wu and Wang, 2011, Frouin et al., 2013). Therefore, without

484   considering the size of the organisms (which is also an important factor in the accumulation

485   of contaminants in biota, in particular, phytoplankton), we can assume that the concentrations

486   of organic contaminants in zooplankton of stations St1, St2, St9 and St11 (which contains

487   more lipids and proteins) may be higher than those in the zooplankton of stations St3, St4 and

488   St17 (which have less lipids and proteins). The biochemical content of the plankton size

489   fractions can change due to variations of the composition of the plankton community and the

490   nutrient inputs linked to the physical and chemical environment, thus affecting the entire

491   trophodynamics of the ecosystem (Chen et al., 2019, 2021; Tedetti et al., 2023).

493

494   **4.2. Plankton total energy amount (E_{TS})**

495   The E_T decreased with size due to plankton biomass reduction with size. In our study, the E_T

496   in SPM_{DW} were lower than previously measured in other areas (Mayzaud et al., 1989; Fabiano

497   et al., 1999; Kim et al., 2019). This is most likely due to the lower phytoplankton biomass

498   reported in the oligotrophic Mediterranean Sea, highlighting their low qualitative values even

499   if spatial and seasonal variations may occur. In the eastern Mediterranean basin, the E_i

500   measured in zooplankton by Danovaro et al., (2000) were even lower than in our study,

501   probably related to higher oligotrophy in their study area. In the Bay of Marseille, the E_T

502   measured at St4 were higher for us than those recorded in similar zooplankton size-fractions

503   during the same season in 2017 by Chen et al. (2019). Plankton showed higher E_{TS} at St1, St4,

504   St9 and St19. At these stations, where bloom conditions prevailed, trophic regimes were

505   probably responsible for enhanced biomass (Mayot et al., 2017; Chen et al., 2019; Tedetti et

506   al., 2023) (Table S1), which may have impacted their E_{TS}. The 0.7–2.7, 2.7–20, and 200–500-

507   µm size-fractions represented the largest energetic reservoir in the Mediterranean phyto-, and

508   zooplankton compartments. Our study highlights their importance as major potential sources

509   of contaminants for their consumers.

510

4.3. Plankton stable isotopes ratios and composition

The fractions comprised between 0.7 and 60 µm corresponded to SPM_{DW} made up of a complex mixture of living, detrital and lithogenic material, difficult to separate (Lam et al., 2015; Tedetti et al., 2023). The main limitation of food web studies relying of stable isotope ratios is to establish an acceptable baseline, using samples mainly composed of primary producers (Harmelin-Vivien et al., 2008; Tamelander et al., 2009). In our study, pico- and nanoplankton dominated the SPM_{DW} biomass which was composed of around 86% of photosynthetic organisms, as confirmed by cytometry results (Boudriga et al., 2022). Moreover, their low C:N ratios suggest a composition dominated by living photosynthetic organisms.

Few studies have measured isotopic compositions of the smallest size-fractions of plankton (Wainright and Fry, 1994; Tamelander et al., 2009), and even fewer have separated them by size (Rau et al., 1990; Rolff, 2000; Im et al., 2015; Hunt et al., 2017; Décima, 2022). The size-fractions from 0.7 to 60 µm (without considering the 0.7–60 µm fraction) have similar $\delta^{13}C$ values but their $\delta^{15}N$ values are rather low (–23.9 ± 0.2 ‰ and 1.4 ± 0.16 ‰, respectively) compared to those measured in other oceanic basins (from –28 to –17 ‰ and from 1 to 12 ‰, respectively) (Wainright and Fry, 1994; Rolff, 2000; Tamelander et al., 2009) and in the Mediterranean Sea (from –25 to –22 ‰ and from 1 to 6 ‰, respectively) (Rau et al., 1990; Harmelin-Vivien et al., 2008; Hunt et al., 2017; Liénart et al., 2017). Several processes may explain the low $\delta^{15}N$ values of the plankton in our study: 1) in the convection areas subjected to algae blooms (such as St9), nutrients made of light isotopes are preferentially uptaken by phytoplankton (Wainright and Fry, 1994; Rolff, 2000; Tamelander et al., 2009), 2) in water with poor nutrient content, ammonium, the main nitrogen source emitted through excretion and recycling, has lower $\delta^{15}N$ values (Checkely and Miller, 1989), and 3) the high proportion of diazotrophs (atmospheric nitrogen fixer) in oligotrophic waters may lower $\delta^{15}N$ values (Pantoja et al., 2002; Montoya et al., 2002; Koppelmann et al., 2003). Within the 0.7 and 60 µm size-fractions, $\delta^{13}C$ and $\delta^{15}N$ values significantly increased with size from pico-, nano- to microplankton, similar to previous studies (Im et al., 2015; Hunt et al., 2017). Differences between primary producers can be related to differences in the isotopic composition of inorganic nitrogen sources and/or fractionation between molecules made of heavy and light isotopes during physiological processes (Ostrom and Fry, 1993). A large contribution of cyanobacteria, mainly composed of *Synechococcus* spp. may lower $\delta^{13}C$ and $\delta^{15}N$ values of SPM in the 0.7–2.7 µm size-fraction (Rau et al., 1990; Rolff, 2000; Hunt et al., 2017). These differences in the composition may also suggest predation within the 0.7–60 µm

545   fraction (Onodera et al., 2018; Armengol et al., 2019). However, an increase in δ^{15}N values

546   with the size has already been observed in autotrophs (Karsh et al., 2003; Hunt et al., 2017).

547   The group composed of size-fractions larger than 60 µm and dominated by zooplankton,

548   mainly copepods (Fierro-González et al., 2023), presented higher δ^{13}C and δ^{15}N values than

549   phytoplankton.

550   The isotopic compositions reported here for the 200–500 µm size-fractions (–22.6 ± 0.4 ‰

551   and 3.2 ± 0.2 ‰, for δ^{13}C and δ^{15}N, respectively) were rather in the lower range of previous

552   estimates in different oceanic basins (from –22 to –19‰ and from 2 to 8‰ for δ^{13}C and δ^{15}N

553   values, respectively) (Fry and Quiñones, 1994; Bode et al., 2007; Yang et al., 2017). Overall,

554   the isotopic compositions measured in the different zooplankton size-fractions were within

555   the same range as those reported in the ultra-oligotrophic eastern Mediterranean basin

556   (Koppelmann et al., 2009; Denda and Christiansen, 2010) and in the more productive area of

557   the Gulf of Lion (Espinasse et al., 2014; Bǎnaru et al., 2014; Hunt et al., 2017).

558   Within the zooplankton size-fractions, δ^{15}N values increased with size, up to the 1000–2000

559   µm fraction, underlining an enhancement of the predation with size (Fry and Quiñones, 1994;

560   Rolff, 2000; Bǎnaru et al., 2014; Espinasse et al., 2014; Hunt et al., 2017). The δ^{15}N values

561   increased with the size-fractions, which may be due to the succession of the different life

562   stages of copepods, coinciding with the pattern observed in their biochemical composition

563   (Espinasse et al., 2014; Chen et al., 2019) related to metabolic changes during the lifespan

564   (Guisande, 2006), adaptative foraging (Kozak et al., 2020), ontogenetics (Mauchline, 1998;

565   Im et al., 2015) or all these processes combined. Fierro-González et al. (2023) reported an

566   increase in the proportion of carnivores with size. However, in the largest size-fraction (>

567   2000 µm), gelatinous organisms were generally overrepresented with respect to other

568   fractions, leading to higher δ^{13}C and lower δ^{15}N values due probably to distinct food sources

569   from smaller fractions (Bǎnaru et al., 2014; Espinasse et al., 2014).

570

571   **4.4. Spatial variation in plankton isotopic compositions**

572   The highest δ^{15}N values in phytoplankton were recorded at St4, located in the Bay of

573   Marseille, which is highly impacted by anthropogenic and terrestrial inputs. These inputs may

574   induce, in case of declining nitrates related to intense bloom events, an increase of the δ^{15}N

575   values (Raimbault et al., 2008; Fey et al., 2021). Moreover, the effluents of the Marseille

576   sewage treatment plant may be ^{15}N-enriched in the inorganic nitrogen pool due to bacterial

577   denitrification (Wainright and Fry, 1994; Cabana and Rasmussen, 1996). The high δ^{13}C

578   values measured in phyto- and zooplankton in the Bay of Marseille (St3 and St4) and in the

579 Gulf of Gabès (St17 and St19) may be due to higher growth rates and nutrient availability in

580 these productive areas (Laws et al., 1995; Bidigare et al., 1997), as well as to inputs of

581 sedimentary organic matter in the water column during sediment resuspension events (Table

582 S1). Moreover, the low $\delta^{15}N$ values measured on the Tunisian coasts support this hypothesis

583 and may be related to seagrass detritus (Cresson et al., 2012). St9, located at the border of the

584 convective area of the Northwestern Mediterranean Sea, was characterized by a post-bloom

585 event during the campaign (Tedetti et al., 2023) and displayed the lowest $\delta^{15}N$ values in

586 phyto- and zooplanktonic organisms. The highest C:N measured at this station may suggest a

587 higher detrital organic matter content and a higher microbial production of regenerated

588 isotopically lighter ammonium compared to the other stations (Maguer et al., 2000).

589 The relatively high $\delta^{13}C$ (and $\delta^{15}N$) values measured in phyto- and zooplankton in the Bay of

590 Marseille and the Gulf of Gabès may also be related to various inputs (sediment resuspension,

591 effluents, etc.), and be the sign of higher levels of contaminants which could derive from the

592 same sources. To support this hypothesis, higher trace metal concentrations have been

593 reported in these coastal stations compared to other MERITE-HIPPOCAMPE stations

594 (Chifflet et al., 2023).

595

596 **4.5. Trophic levels and food web implications**

597 The TLs determined in this study, ranging from 1.5 to 3.6, increased with size and spread out

598 over 2 TLs. TLs lower than 2 may be related to a mixture of primary producers and

599 consumers mainly found at some stations in the 60–200 µm size-fraction, related to clogging

600 of the sampling device caused by phytoplankton. Further improvements in sampling methods

601 by using larger mesh-size nets for zooplankton size-fractions collection may avoid potential

602 clogging during bloom events and the presence of phytoplankton within the 60–200 µm size-

603 fraction.

604 When biomass is averaged to the TL of zooplankton (TL_B), higher values are obtained at the

605 coastal (St2, and St3), and offshore (St9, St10, and St11) stations. High adaptability in food

606 habits of zooplankton is well known and omnivory seems to be the most common trophic

607 pathway (Fierro-González et al., 2023). Higher TLs are generally reached in microbial food

608 webs, often observed in oligotrophic regimes (Søreide et al., 2006; Kürten et al., 2013). St10

609 and St11 contained carnivorous plankton, such as chaetognaths which may explain the higher

610 TLs of the zooplankton community observed in these areas (Fierro-González et al., 2023). It

611 has been suggested that the TFF between phytoplankton and protozoans is equal to 0,

612 contributing to an underestimation of the number of TLs in planktonic food webs (Gutiérrez-

613 Rodríguez et al., 2014). However, in this work, we suggest that the higher TLs of plankton
614 were probably related to the microbial food web.

615 Coastal stations (St1, St4, St15, St17 and St19) were characterized by lower TL_B. The
616 lower TL of plankton in productive systems is classic in herbivore food webs, dominated by
617 larger phytoplankton organisms readily available to zooplankton (Sommer et al., 2002;
618 Fileman et al., 2007). Food chain length decreases in productive ecosystems due to an
619 adaptive foraging of consumers which selects the most abundant low TL resources (Kondoh
620 and Ninomiya, 2009). Detritus and phytoplankton were dominant in these stations in the 60–
621 200 µm size-fraction contributing to lowering TL_B values (Fierro-González et al., 2023).

622 In addition, the zooplankton biomass was related to the trophic pathways. A negative
623 relationship between the TL_B and the zooplankton biomass was observed during this study.
624 Higher biomasses of zooplankton have been measured at coastal stations relative to offshore
625 areas in relation to their primary production (Champalbert, 1996). Where TLs were high (St9,
626 St10 and St11), large size fractions (500–1000 and 1000–2000 µm) were also well
627 represented, accounting for 27 to 54% of the total zooplankton biomass. Espinasse et al.
628 (2014) have already highlighted the overrepresentation of large plankton organisms in
629 moderately productive areas, while Décima (2022) have reported an inverse relationship
630 between food chain length and productivity in zooplankton. Although located in the offshore
631 area, St9 was characterized by a still productive post-bloom situation (Tedetti et al., 2023)
632 with high TL_B. Usually, during post-bloom, diatoms give way to inedible algae not consumed
633 by zooplankton organisms and the source of organic matter is obtained through the cell lysis,
634 fuelling microbial loop and enhancing food steps (Sommer et al., 2002). High C:N ratios
635 observed at St9 may indicate heterotrophy within the 0.7–60 µm fractions (Harmelin-Vivien
636 et al., 2008). The post-bloom situation may induce a decrease of the resources and thus
637 mesoplankton preying on microplankton (Levinsen et al., 2000; Basedow et al., 2016). Hence,
638 the results reported here highlight different trophodynamic scenarios in the Mediterranean
639 plankton food webs and their control on planktonic biomasses, as hypothesized by Fry and
640 Quiñones (1994).
641 Contrasting carbon fluxes can impact contaminant transfer. The ability of each contaminant to
642 bioaccumulate can lead to different scenarios. In low-productive ecosystems, organic matter
643 fluxes go through more trophic steps, which can favor a higher transfer of contaminants that
644 will bioaccumulate such as methylmercury, PCBs or Cd (Tiano et al., 2014; Schartup et al.,
645 2018; Chouvelon et al., 2019). Conversely, in productive ecosystems, direct access to organic
646 matter sources and reduced food steps favors higher transfer of contaminants with little or no

647 capacity to bioaccumulate, such as the numerous trace elements Co, Ni, Cu, Ag, Pb, and Zn

648 (Chouvelon et al., 2019).

649

650   **4.6. Plankton food web flows**

651 The difference in stable isotope composition between phytoplankton size-fractions made them

652 relevant candidates for mixing model analysis of their relative contributions to zooplankton

653 biomass (Phillips et al., 2014; Hunt et al., 2017). Overall, the contribution of the 0.7–2.7-µm

654 size-fraction to the diet of the 60–500 µm size fraction underlines the role of the

655 microzooplankton (60–200 µm) and of the small mesozooplankton (200–500 µm) in the

656 transfer of organic matter from the baseline to higher trophic level consumers. The

657 picoplankton size fraction was mainly composed of *Synechococcus* spp., the most abundant

658 phytoplankton organism in the Mediterranean Sea that sustains primary production (Boudriga

659 et al., 2022). In fact, during the MERITE-HIPPOCAMPE campaign, picoplankton accounted

660 for, on average, 27% of the total biomass of phytoplankton.

661 Classically, we consider that nanoflagellates and microzooplankton (from 2 to 200 µm size-

662 fractions) may represent intermediate food steps (Ryther, 1969; Calbet and Landry, 1999)

663 ensuring the link between the 0.7–2.7 µm fraction and mesozooplankton (200–2000 µm)

664 (Sommer et al., 2000). The 60 to 500 µm size-fractions were constituted of a large percentage

665 of phytoplankton and detritus that would have contributed to lowering their stable isotope

666 ratios. This may have consequences with regard to the mixing model results and may explain

667 the high percentage of picoplankton estimated in the diet of 60–500 µm size-fraction.

668 However, in agreement with our results, and despite their small size, recent studies

669 demonstrated that small copepods may feed on picoplankton (Motwani and Gorokhova, 2013;

670 Im et al., 2015; Major et al., 2017).

671 Primary producers were also dominant in the 2.7–20 µm fractions, representing 69% of the

672 phytoplanktonic biomass and about half of the total food supply to both the 60–500 and the

673 500–2000 µm size-fractions. Nanoplankton was mainly composed of nanoeukaryotes and its

674 contribution to the planktonic food web seems essential, in agreement with the results of Hunt

675 et al. (2017). Finally, the 20–60 µm fraction has low biomass and represents an important

676 contribution only to the diet of the > 2000 µm size-fractions. TFFs for plankton should be

677 experimentally determined and a higher number of replicates should be analyzed to improve

678 model results and to reduce their variability.

679 Differences in contaminant accumulation have been reported in phytoplankton size-fractions.

680 Trace metals reflected, for each element, contrasted accumulation patterns between small and

681   large phytoplankton fractions (Chifflet et al., 2023). Higher methylmercury concentrations

682   were reported during a picoplanktonic bloom, probably due to a higher surface to volume

683   ratio, favoring uptake (Heimbürger et al., 2010). In addition, for PCBs, a higher accumulation

684   was observed in smaller cells (Axelman et al., 1997). The different carbon size-fractions of

685   food sources can thus influence the transfer of contaminants and concentrations in

686   zooplankton consumers.

687

5. Conclusions

689   During the MERITE-HIPPOCAMPE campaign, plankton size-fractions revealed contrasted

690   biochemical and isotopic compositions related to their size, composition and location.

691   Carbohydrate concentrations were the highest in phytoplankton (between 0.7 and 60 µm size-

692   fractions) with respect to zooplankton (> 60 µm size-fractions), which displayed high protein

693   and lipid contents increasing with size. The affinity of proteins and lipids for contaminants

694   makes zooplankton more sensitive to their accumulation (regardless of the size of organisms).

695   Due to the high amount of energy contained in their biomass, the pico- and nanoplankton

696   represents a major food resource in Mediterranean ecosystems fueling the zooplankton food

697   webs and an essential pathway for contaminants due to the combination of small size and high

698   energetic content. In the zooplankton community, the 200–500 µm size-fraction, dominated

699   by copepods, showed the highest energy amount, which explains their role as essential food

700   resource for many planktivorous fishes. Spatial variations of isotopic compositions of

701   plankton size-fractions were also observed, revealing different carbon sources between the

702   coast and the offshore areas, and between the Bay of Gabès (southern coast) and the Bay of

703   Toulon (northern coast), and resulting in a different exposure to contaminants. Trophic levels

704   revealed increasing predation with size, which can result in the biomagnification of

705   contaminants. Trophic pathways in planktonic food webs displayed spatial variations

706   influenced by the availability of phytoplankton resources. Higher predation occurred in low

707   productive areas where the zooplankton community reached the highest mean trophic levels,

708   increasing the potential exposure of planktonic food webs to contaminants. Our findings on

709   the spatial variations of the biomass, biochemical composition, and the role of the different

710   plankton size-fractions in the food web, as well as the different flows of organic matter in the

711   pelagic food webs, are an essential step for the comprehension of the transfer of contaminants

712   in the Mediterranean pelagic food webs.

713

714

Author contribution statement

Conception and design of study: DB, MT, FC, MP,

Acquisition of data: JATO, MeTe, LG, PF, BL, GG, IB, MB, AZ, MT, SC

Analysis and/or interpretation of data: JATO, DB, MT, TG, CC, SC

Drafting of the manuscript: JATO, DB, MT

Revising/editing of the manuscript: JATO, DB, MT, FC, BL

Project administration and funding acquisition: DB, MT, FC, MP

Supplementary information

Supplementary material related to this article is available online at: xxx

References

Alekseenko, E., Thouvenin, B., Tronczyński, J., Carlotti, F., Garreau, P., Tixier, C., Baklouti, M., 2018. Modeling of PCB trophic transfer in the Gulf of Lions; 3D coupled model

748   application. Marine Pollution Bulletin 128, 140–155.

749   https://doi.org/10.1016/j.marpolbul.2018.01.008

750 Armengol, L., Calbet, A., Franchy, G., Rodríguez-Santos, A., Hernández-León, S., 2019.

751   Planktonic food web structure and trophic transfer efficiency along a productivity

752   gradient in the tropical and subtropical Atlantic Ocean. Scientific Reports 9, 2044.

753   https://doi.org/10.1038/s41598-019-38507-9

754 Axelman, J., Broman, D., Näf, C., 1997. Field Measurements of PCB Partitioning between

755   Water and Planktonic Organisms: Influence of Growth, Particle Size, and

756   Solute−Solvent Interactions. Environmental Science & Technology 31, 665–669.

757   https://doi.org/10.1021/es960088+

758 Bănaru, D., Carlotti, F., Barani, A., Grégori, G., Neffati, N., Harmelin-Vivien, M., 2014.

759   Seasonal variation of stable isotope ratios of size-fractionated zooplankton in the Bay of

760   Marseille (NW Mediterranean Sea). Journal of Plankton Research 36, 145–156.

761   https://doi.org/10.1093/plankt/fbt083

762 Bănaru, D., Diaz, F., Verley, P., Campbell, R., Navarro, J., Yohia, C., Oliveros-Ramos, R.,

763   Mellon-Duval, C., Shin, Y.-J., 2019. Implementation of an end-to-end model of the Gulf

764   of Lions ecosystem (NW Mediterranean Sea). I. Parameterization, calibration and

765   evaluation. Ecological Modelling 401, 1–19.

766   https://doi.org/10.1016/j.ecolmodel.2019.03.005

767 Bănaru, D., Mellon-Duval, C., Roos, D., Bigot, J.-L., Souplet, A., Jadaud, A., Beaubrun, P.,

768   Fromentin, J.-M., 2013. Trophic structure in the Gulf of Lions marine ecosystem (north-

769   western Mediterranean Sea) and fishing impacts. Journal of Marine Systems 111–112,

770   45–68. https://doi.org/10.1016/j.jmarsys.2012.09.010

771 Banse, K., Mosher, S., 1980. Adult Body Mass and Annual Production/Biomass Relationships

772   of Field Populations. Ecological Monographs 50, 355–379.

773   https://doi.org/10.2307/2937256

774 Basedow, S.L., de Silva, N.A.L., Bode, A., van Beusekorn, J., 2016. Trophic positions of

775   mesozooplankton across the North Atlantic: estimates derived from biovolume spectrum

776   theories and stable isotope analyses. Journal of Plankton Research 38, 1364–1378.

777   https://doi.org/10.1093/plankt/fbw070

778 Bhat, K.L., Rayadurga, S., Ansari, Z.A., 1993. Biochemical composition of zooplankton from

779   the northern Arabian Sea. Pakistan Journal of Marine Sciences 2, 17-22.

780 Bidigare, R.R., Fluegge, A., Freeman, K.H., Hanson, K.L., Hayes, J.M., Hollander, D.,

781   Jasper, J.P., King, L.L., Laws, E.A., Milder, J., Millero, F.J., Pancost, R., Popp, B.N.,

782   Steinberg, P.A., Wakeham, S.G., 1997. Consistent fractionation of 13C in nature and in
783   the laboratory: Growth-rate effects in some haptophyte algae. Global Biogeochemical
784   Cycles 11, 279–292. https://doi.org/10.1029/96GB03939

785   Bishop, J.K.B., Edmond, J.M., Ketten, D.R., Bacon, M.P., Silker, W.B., 1977. The chemistry,
786   biology, and vertical flux of particulate matter from the upper 400 m of the equatorial
787   Atlantic Ocean. Deep Sea Research 24, 511–548. https://doi.org/10.1016/0146-
788   6291(77)90526-4

789   Bishop, J.K.B., Lam, P.J., Wood, T.J., 2012. Getting good particles: Accurate sampling of
790   particles by large volume in-situ filtration: Getting good particles. Limnology and
791   Oceanography: Methods 10, 681–710. https://doi.org/10.4319/lom.2012.10.681

792   Bligh, E.G., Dyer, W.J., 1959. A rapid method of total lipid extraction and purification.
793   Canadian Journal of Biochemistry and Physiology 37, 911–917.
794   https://doi.org/10.1139/o59-099

795   Bode, A., Alvarez-Ossorio, M.T., Cunha, M.E., Garrido, S., Peleteiro, J.B., Porteiro, C.,
796   Valdés, L., Varela, M., 2007. Stable nitrogen isotope studies of the pelagic food web on
797   the Atlantic shelf of the Iberian Peninsula. Progress in Oceanography, 74, 115–131.
798   https://doi.org/10.1016/j.pocean.2007.04.005

799   Boudriga, I., Thyssen, M., Zouari, A., Garcia, N., Tedetti, M., Bel Hassen, M., 2022.
800   Ultraphytoplankton community structure in subsurface waters along a North-South
801   Mediterranean transect. Marine Pollution Bulletin 182, 113977.
802   https://doi.org/10.1016/j.marpolbul.2022.113977

803   Brown, J.H., Gillooly, J.F., Allen, A.P., Savage, V.M., West, G.B., 2004. Toward a Metabolic
804   Theory of Ecology. Ecology 85, 1771–1789. https://doi.org/10.1890/03-9000

805   Cabana, G., Rasmussen, J.B., 1994. Modelling food chain structure and contaminant
806   bioaccumulation using stable nitrogen isotopes. Nature 372, 255–257.
807   https://doi.org/10.1038/372255a0

808   Cabana, G., Rasmussen, J.B., 1996. Comparison of aquatic food chains using nitrogen
809   isotopes. Proceedings of the National Academy of Sciences 93, 10844–10847.
810   https://doi.org/10.1073/pnas.93.20.10844

811   Calbet, A., Landry, M.R., 1999. Mesozooplankton influences on the microbial food web:
812   Direct and indirect trophic interactions in the oligotrophic open ocean. Limnology and
813   Oceanography 44, 1370–1380. https://doi.org/10.4319/lo.1999.44.6.1370

814   Carlotti, F., Thibault-Botha, D., Nowaczyk, A., Lefèvre, D., 2008. Zooplankton community
815   structure, biomass and role in carbon fluxes during the second half of a phytoplankton

816   bloom in the eastern sector of the Kerguelen Shelf (January–February 2005). Deep Sea

817   Research Part II: Topical Studies in Oceanography, 55, 720–733.

818   https://doi.org/10.1016/j.dsr2.2007.12.010

819   Champalbert, G., 1996. Characteristics of zooplankton standing stock and communities in the

820   western Mediterranean Sea: relations to hydrology. Scientia Marina 60, 97–113.

821   Checkley, D.M., Miller, C.A., 1989. Nitrogen isotope fractionation by oceanic zooplankton.

822   Deep Sea Research Part A. Oceanographic Research Papers 36, 1449–1456.

823   https://doi.org/10.1016/0198-0149(89)90050-2

824   Chen, C.-T., Bǎnaru, D., Carlotti, F., Faucheux, M., Harmelin-Vivien, M., 2019. Seasonal

825   variation in biochemical and energy content of size-fractionated zooplankton in the Bay

826   of Marseille (North-Western Mediterranean Sea). Journal of Marine Systems 199,

827   103223. https://doi.org/10.1016/j.jmarsys.2019.103223

828   Chen, C.-T., Carlotti, F., Harmelin-Vivien, M., Guilloux, L., Bǎnaru, D., 2021. Temporal

829   variation in prey selection by adult European sardine (Sardina pilchardus) in the NW

830   Mediterranean Sea. Progress in Oceanography 196, 102617.

831   https://doi.org/10.1016/j.pocean.2021.102617

832   Chen, C.-T., Carlotti, F., Harmelin-Vivien, M., Lebreton, B., Guillou, G., Vassallo, L., Le

833   Bihan, M., Bǎnaru, D., 2022. Diet and trophic interactions of Mediterranean

834   planktivorous fishes. Marine Biology 169, 119. https://doi.org/10.1007/s00227-022-

835   04103-1

836   Chifflet, S., Briant, N., Tesán-Onrubia, J.A., Zaaboub, N., Amri, S., Radakovitch, O., Bǎnaru,

837   D., Tedetti, M., 2023. Distribution and accumulation of trace metal in the planktonic food

838   web of the Mediterranean Sea (MERITE-HIPPOCAMPE campaign). Marine Pollution

839   Bulletin 186, 114384. https://doi.org/10.1016/j.marpolbul.2022.114384.

840   Chouvelon, T., Strady, E., Harmelin-Vivien, M., Radakovitch, O., Brach-Papa, C., Crochet,

841   S., Knoery, J., Rozuel, E., Thomas, B., Tronczynski, J., Chiffoleau, J.-F., 2019. Patterns

842   of trace metal bioaccumulation and trophic transfer in a phytoplankton-zooplankton-small

843   pelagic fish marine food web. Marine Pollution Bulletin 146, 1013–1030.

844   https://doi.org/10.1016/j.marpolbul.2019.07.047

845   Cohen, J.E., Pimm, S.L., Yodzis, P., Saldana, J., 1993. Body Sizes of Animal Predators and

846   Animal Prey in Food Webs. The Journal of Animal Ecology 62, 67.

847   https://doi.org/10.2307/5483

848   Cossa, D., Knoery, J., Bǎnaru, D., Harmelin-Vivien, M., Sonke, J.E., Hedgecock, I.M., Bravo,

849   A.G., Rosati, G., Canu, D., Horvat, M., Sprovieri, F., Pirrone, N., Heimbürger-Boavida,

850   L.-E., 2022. Mediterranean Mercury Assessment 2022: An Updated Budget, Health

851   Consequences, and Research Perspectives. Environmental Science & Technology 56,

852   3840–3862. https://doi.org/10.1021/acs.est.1c03044

853 Cresson, P., Ruitton, S., Fontaine, M.-F., Harmelin-Vivien, M., 2012. Spatio-temporal

854   variation of suspended and sedimentary organic matter quality in the Bay of Marseilles

855   (NW Mediterranean) assessed by biochemical and isotopic analyses. Marine Pollution

856   Bulletin 64, 1112–1121. https://doi.org/10.1016/j.marpolbul.2012.04.003

857 Cresson, P., Chouvelon, T., Bustamante, P., Bănaru, D., Baudrier, J., Le Loc'h, F., Mauffret,

858   A., Mialet, B., Spitz, J., Wessel, N., Briand, M.J., Denamiel, M., Doray, M., Guillou, G.,

859   Jadaud, A., Lazard, C., Prieur, S., Rouquette, M., Saraux, C., Serre, S., Timmerman, C.-

860   A., Verin, Y., Harmelin-Vivien, M., 2020. Primary production and depth drive different

861   trophic structure and functioning of fish assemblages in French marine ecosystems.

862   Progress in Oceanography 186, 102343. https://doi.org/10.1016/j.pocean.2020.102343

863 Danovaro, R., Dell'Anno, A., Pusceddu, A., Marrale, D., Della Croce, N., Fabiano, M.,

864   Tselepides, A., 2000. Biochemical composition of pico-, nano- and micro-particulate

865   organic matter and bacterioplankton biomass in the oligotrophic Cretan Sea (NE

866   Mediterranean). Progress in Oceanography 46, 279–310. https://doi.org/10.1016/S0079-

867   6611(00)00023-9

868 Décima, M., 2022. Zooplankton trophic structure and ecosystem productivity. Marine

869   Ecology Progress Series 692, 23–42. https://doi.org/10.3354/meps14077

870 Denda, A., Christiansen, B., 2010. Zooplankton at a seamount in the eastern Mediterranean:

871   distribution and trophic interactions. Journal of the Marine Biological Association of the

872   United Kingdom 91, 33–49. https://doi.org/10.1017/S0025315410001153

873 DuBois, Michel., Gilles, K.A., Hamilton, J.K., Rebers, P.A., Smith, Fred., 1956. Colorimetric

874   Method for Determination of Sugars and Related Substances. Analytical Chemistry 28,

875   350–356. https://doi.org/10.1021/ac60111a017

876 Durrieu de Madron, X., Guieu, C., Sempéré, R., Conan, P., Cossa, D., D'Ortenzio, F.,

877   Estournel, C., Gazeau, F., Rabouille, C., Stemmann, L., Bonnet, S., Diaz, F., Koubbi, P.,

878   Radakovitch, O., Babin, M., Baklouti, M., Bancon-Montigny, C., Belviso, S.,

879   Bensoussan, N., Bonsang, B., Bouloubassi, I., Brunet, C., Cadiou, J.-F., Carlotti, F.,

880   Chami, M., Charmasson, S., Charrière, B., Dachs, J., Doxaran, D., Dutay, J.-C., Elbaz-

881   Poulichet, F., Eléaume, M., Eyrolles, F., Fernandez, C., Fowler, S., Francour, P.,

882   Gaertner, J.C., Galzin, R., Gasparini, S., Ghiglione, J.-F., Gonzalez, J.-L., Goyet, C.,

883   Guidi, L., Guizien, K., Heimbürger, L.-E., Jacquet, S.H.M., Jeffrey, W.H., Joux, F., Le

Hir, P., Leblanc, K., Lefèvre, D., Lejeusne, C., Lemé, R., Loÿe-Pilot, M.-D., Mallet, M., Méjanelle, L., Mélin, F., Mellon, C., Mérigot, B., Merle, P.-L., Migon, C., Miller, W.L., Mortier, L., Mostajir, B., Mousseau, L., Moutin, T., Para, J., Pérez, T., Petrenko, A., Poggiale, J.-C., Prieur, L., Pujo-Pay, M., Pulido-Villena, Raimbault, P., Rees, A.P., Ridame, C., Rontani, J.-F., Ruiz Pino, D., Sicre, M.A., Taillandier, V., Tamburini, C., Tanaka, T., Taupier-Letage, I., Tedetti, M., Testor, P., Thébault, H., Thouvenin, B., Touratier, F., Tronczynski, J., Ulses, C., Van Wambeke, F., Vantrepotte, V., Vaz, S., Verney, R., 2011. Marine ecosystems' responses to climatic and anthropogenic forcings in the Mediterranean. Progress in Oceanography 91, 97–166. https://doi.org/10.1016/j.pocean.2011.02.003

Espinasse, B., Harmelin-Vivien, M., Tiano, M., Guilloux, L., Carlotti, F., 2014. Patterns of variations in C and N stable isotope ratios in size-fractionated zooplankton in the Gulf of Lion, NW Mediterranean Sea. Journal of Plankton Research 36, 1204–1215. https://doi.org/10.1093/plankt/fbu043

Fabiano, M., Danovaro, R., Povero, P., 1999. Vertical Distribution and Biochemical Composition of Pico- and Microparticulate Organic Matter in the Ross Sea (Antarctica), in: Spezie, G., Manzella, G.M.R. (Eds.), Oceanography of the Ross Sea Antarctica. Springer Milan, Milano, pp. 233–246. https://doi.org/10.1007/978-88-470-2250-8_16

Fan, C.-W., Reinfelder, J.R., 2003. Phenanthrene Accumulation Kinetics in Marine Diatoms. Environmental Science & Technology 37, 3405–3412. https://doi.org/10.1021/es026367g

Fey, P., Parravicini, V., Bănaru, D., Dierking, J., Galzin, R., Lebreton, B., Meziane, T., Polunin, N.V.C., Zubia, M., Letourneur, Y., 2021. Multi-trophic markers illuminate the understanding of the functioning of a remote, low coral cover Marquesan coral reef food web. Scientific Reports 11, 20950. https://doi.org/10.1038/s41598-021-00348-w

Fierro-González, P., Pagano, M., Guilloux, L., Makhlouf, N., Tedetti, M., Carlotti, F., 2023. Zooplankton biomass, size structure, and associated metabolic fluxes with focus on its roles at the chlorophyll maximum layer during the plankton-contaminant MERITE-HIPPOCAMPE cruise. Submitted to this special issue.

Fileman, E., Smith, T., Harris, R., 2007. Grazing by Calanus helgolandicus and Para-Pseudocalanus spp. on phytoplankton and protozooplankton during the spring bloom in the Celtic Sea. Journal of Experimental Marine Biology and Ecology 348, 70–84. https://doi.org/10.1016/j.jembe.2007.04.003

Frouin, H., Dangerfield, N., Macdonald, R.W., Galbraith, M., Crewe, N., Shaw, P., Mackas, D., Ross, P.S., 2013. Partitioning and bioaccumulation of PCBs and PBDEs in marine

918   plankton from the Strait of Georgia, British Columbia, Canada. Progress in

919   Oceanography, Strait of Georgia Ecosystem Research Initiative (ERI) 115, 65–75.

920   https://doi.org/10.1016/j.pocean.2013.05.023

921 Fry, B., Quiñones, R.B., 1994. Biomass spectra and stable isotope indicators of trophic level

922   in zooplankton of the northwest Atlantic. Marine Ecology Progress Series 112, 201–204.

923 Guisande, C., 2006. Biochemical fingerprints in zooplankton. Limnetica 25, 369–376.

924 Gutiérrez-Rodríguez, A., Décima, M., Popp, B.N., Landry, M.R., 2014. Isotopic invisibility of

925   protozoan trophic steps in marine food webs. Limnology and Oceanography 59, 1590–

926   1598. https://doi.org/10.4319/lo.2014.59.5.1590

927 Harmelin-Vivien, M., Bănaru, D., Dromard, C.R., Ourgaud, M., Carlotti, F., 2019.

928   Biochemical composition and energy content of size-fractionated zooplankton east of the

929   Kerguelen Islands. Polar Biology 42, 603–617. https://doi.org/10.1007/s00300-019-

930   02458-8

931 Harmelin-Vivien, M., Loizeau, V., Mellon, C., Beker, B., Arlhac, D., Bodiguel, X., Ferraton,

932   F., Hermand, R., Philippon, X., Salen-Picard, C., 2008. Comparison of C and N stable

933   isotope ratios between surface particulate organic matter and microphytoplankton in the

934   Gulf of Lions (NW Mediterranean). Continental Shelf Research, 28, 1911–1919.

935   https://doi.org/10.1016/j.csr.2008.03.002

936 Heimbürger, L.-E., Cossa, D., Marty, J.-C., Migon, C., Averty, B., Dufour, A., Ras, J., 2010.

937   Methyl mercury distributions in relation to the presence of nano- and picophytoplankton

938   in an oceanic water column (Ligurian Sea, North-western Mediterranean). Geochimica et

939   Cosmochimica Acta 74, 5549–5559. https://doi.org/10.1016/j.gca.2010.06.036

940 Hirst, A.G., Kiørboe, T., 2002. Mortality of marine planktonic copepods: global rates and

941   patterns. Marine Ecology Progress Series 230, 195–209.

942   https://doi.org/10.3354/meps230195

943 Hunt, B.P.V., Carlotti, F., Donoso, K., Pagano, M., D'Ortenzio, F., Taillandier, V., Conan, P.,

944   2017. Trophic pathways of phytoplankton size classes through the zooplankton food web

945   over the spring transition period in the north-west Mediterranean Sea. Journal of

946   Geophysical Research: Oceans 122, 6309–6324. https://doi.org/10.1002/2016JC012658

947 Im, D.-H., Wi, J.H., Suh, H.-L., 2015. Evidence for ontogenetic feeding strategies in four

948   calanoid copepods in the East Sea (Japan Sea) in summer, revealed by stable isotope

949   analysis. Ocean Science Journal 50, 481–490. https://doi.org/10.1007/s12601-015-0044-y

950 Jónasdóttir, S.H., 2019. Fatty Acid Profiles and Production in Marine Phytoplankton. Marine

951   Drugs 17, 151. https://doi.org/10.3390/md17030151

952 Karsh, K.L., Trull, T.W., Lourey, M.J., Sigman, D.M., 2003. Relationship of nitrogen isotope

953   fractionation to phytoplankton size and iron availability during the Southern Ocean Iron

954   RElease Experiment (SOIREE). Limnology and Oceanography 48, 1058–1068.

955   https://doi.org/10.4319/lo.2003.48.3.1058

956 Khammeri, Y., Bellaaj-Zouari, A., Hamza, A., Medhioub, W., Sahli, E., Akrout, F., Barraj,

957   N., Ben Kacem, M.Y., Bel Hassen, M., 2020. Ultraphytoplankton community

958   composition in Southwestern and Eastern Mediterranean Basin: Relationships to water

959   mass properties and nutrients. Journal of Sea Research 158, 101875.

960   https://doi.org/10.1016/j.seares.2020.101875

961 Khammeri, Y., Hamza, I.S., Zouari, A.B., Hamza, A., Sahli, E., Akrout, F., Ben Kacem,

962   M.Y., Messaoudi, S., Hassen, M.B., 2018. Atmospheric bulk deposition of dissolved

963   nitrogen, phosphorus and silicate in the Gulf of Gabès (South Ionian Basin); implications

964   for marine heterotrophic prokaryotes and ultraphytoplankton. Continental Shelf Research

965   159, 1–11. https://doi.org/10.1016/j.csr.2018.03.003

966 Kim, Y., Lee, Jang Han, Kang, J.J., Lee, Jae Hyung, Lee, H.W., Kang, C.K., Lee, S.H., 2019.

967   River discharge effects on the contribution of small-sized phytoplankton to the total

968   biochemical composition of POM in the Gwangyang Bay, Korea. Estuarine, Coastal and

969   Shelf Science 226, 106293. https://doi.org/10.1016/j.ecss.2019.106293

970 Kondoh, M., Ninomiya, K., 2009. Food-chain length and adaptive foraging. Proceedings of

971   the Royal Society B: Biological Sciences 276, 3113–3121.

972   https://doi.org/10.1098/rspb.2009.0482

973 Koppelmann, R., Weikert, H., Lahajnar, N., 2003. Vertical distribution of mesozooplankton

974   and its δ15N signature at a deep-sea site in the Levantine Sea (eastern Mediterranean) in

975   April 1999. Journal of Geophysical Research: Oceans 108.

976   https://doi.org/10.1029/2002JC001351

977 Koppelmann, R., Böttger-Schnack, R., Möbius, J., Weikert, H., 2009. Trophic relationships of

978   zooplankton in the eastern Mediterranean based on stable isotope measurements. Journal

979   of Plankton Research 31, 669–686. https://doi.org/10.1093/plankt/fbp013

980 Kozak, E.R., Franco-Gordo, C., Godínez-Domínguez, E., Suárez-Morales, E., Ambriz-

981   Arreola, I., 2020. Seasonal variability of stable isotope values and niche size in tropical

982   calanoid copepods and zooplankton size fractions. Marine Biology 167, 37.

983   https://doi.org/10.1007/s00227-020-3653-7

984 Krasakopoulou, E., Karageorgis, A.P., 2005. Spatial and temporal distribution patterns of

985   suspended particulate matter and particulate organic carbon in the Saronikos Gulf

986   (eastern Mediterranean, Greece). Geo-Marine Letters 25, 343–359.

987   https://doi.org/10.1007/s00367-005-0007-x

988   Kürten, B., Painting, S.J., Struck, U., Polunin, N.V.C., Middelburg, J.J., 2013. Tracking

989   seasonal changes in North Sea zooplankton trophic dynamics using stable isotopes.

990   Biogeochemistry 113, 167–187. https://doi.org/10.1007/s10533-011-9630-y

991   Lam, P.J., Ohnemus, D.C., Auro, M.E., 2015. Size-fractionated major particle composition

992   and concentrations from the US GEOTRACES North Atlantic Zonal Transect. Deep Sea

993   Research Part II: Topical Studies in Oceanography, 116, 303–320.

994   https://doi.org/10.1016/j.dsr2.2014.11.020

995   Laws, E.A., Popp, B.N., Bidigare, R.R., Kennicutt, M.C., Macko, S.A., 1995. Dependence of

996   phytoplankton carbon isotopic composition on growth rate and [CO2]aq: Theoretical

997   considerations and experimental results. Geochimica et Cosmochimica Acta 59, 1131–

998   1138. https://doi.org/10.1016/0016-7037(95)00030-4

999   Leblanc, K., Quéguiner, B., Diaz, F., Cornet, V., Michel-Rodriguez, M., Durrieu de Madron,

1000   X., Bowler, C., Malviya, S., Thyssen, M., Grégori, G., Rembauville, M., Grosso, O.,

1001   Poulain, J., de Vargas, C., Pujo-Pay, M., Conan, P., 2018. Nanoplanktonic diatoms are

1002   globally overlooked but play a role in spring blooms and carbon export. Nature

1003   Communications 9, 953. https://doi.org/10.1038/s41467-018-03376-9

1004   Levinsen, H., Turner, J.T., Nielsen, T.G., Hansen, B.W., 2000. On the trophic coupling

1005   between protists and copepods in arctic marine ecosystems. Marine Ecology Progress

1006   Series 204, 65–77. https://doi.org/10.3354/meps204065

1007   Liénart, C., Savoye, N., Bozec, Y., Breton, E., Conan, P., David, V., Feunteun, E., Grangeré,

1008   K., Kerhervé, P., Lebreton, B., Lefebvre, S., L'Helguen, S., Mousseau, L., Raimbault, P.,

1009   Richard, P., Riera, P., Sauriau, P.-G., Schaal, G., Aubert, F., Aubin, S., Bichon, S.,

1010   Boinet, C., Bourasseau, L., Bréret, M., Caparros, J., Cariou, T., Charlier, K., Claquin, P.,

1011   Cornille, V., Corre, A.-M., Costes, L., Crispi, O., Crouvoisier, M., Czamanski, M., Del

1012   Amo, Y., Derriennic, H., Dindinaud, F., Durozier, M., Hanquiez, V., Nowaczyk, A.,

1013   Devesa, J., Ferreira, S., Fornier, M., Garcia, F., Garcia, N., Geslin, S., Grossteffan, E.,

1014   Gueux, A., Guillaudeau, J., Guillou, G., Joly, O., Lachaussée, N., Lafont, M.,

1015   Lamoureux, J., Lecuyer, E., Lehodey, J.-P., Lemeille, D., Leroux, C., Macé, E., Maria,

1016   E., Pineau, P., Petit, F., Pujo-Pay, M., Rimelin-Maury, P., Sultan, E., 2017. Dynamics of

1017   particulate organic matter composition in coastal systems: A spatio-temporal study at

1018   multi-systems scale. Progress in Oceanography 156, 221–239.

1019   https://doi.org/10.1016/j.pocean.2017.03.001

1020 Liénart, C., Savoye, N., David, V., Ramond, P., Rodriguez Tress, P., Hanquiez, V., Marieu,
1021   V., Aubert, F., Aubin, S., Bichon, S., Boinet, C., Bourasseau, L., Bozec, Y., Bréret, M.,
1022   Breton, E., Caparros, J., Cariou, T., Claquin, P., Conan, P., Corre, A.-M., Costes, L.,
1023   Crouvoisier, M., Del Amo, Y., Derriennic, H., Dindinaud, F., Duran, R., Durozier, M.,
1024   Devesa, J., Ferreira, S., Feunteun, E., Garcia, N., Geslin, S., Grossteffan, E., Gueux, A.,
1025   Guillaudeau, J., Guillou, G., Jolly, O., Lachaussée, N., Lafont, M., Lagadec, V.,
1026   Lamoureux, J., Lauga, B., Lebreton, B., Lecuyer, E., Lehodey, J.-P., Leroux, C.,
1027   L'Helguen, S., Macé, E., Maria, E., Mousseau, L., Nowaczyk, A., Pineau, P., Petit, F.,
1028   Pujo-Pay, M., Raimbault, P., Rimmelin-Maury, P., Rouaud, V., Sauriau, P.-G., Sultan, E.,
1029   Susperregui, N., 2018. Dynamics of particulate organic matter composition in coastal
1030   systems: Forcing of spatio-temporal variability at multi-systems scale. Progress in
1031   Oceanography 162, 271–289. https://doi.org/10.1016/j.pocean.2018.02.026

1032 Ljungström, G., Claireaux, M., Fiksen, Ø., Jørgensen, C., 2020. Body size adaptions under
1033   climate change: zooplankton community more important than temperature or food
1034   abundance in model of a zooplanktivorous fish. Marine Ecology Progress Series 636, 1–
1035   18. https://doi.org/10.3354/meps13241

1036 Lowry, O.H., Rosebrough, N.J., Farr, A.L., Randall, R.J., 1951. Protein measurement with the
1037   Folin phenol reagent. Journal of Biological Chemistry 193, 265–275.

1038 Maguer, J.-F., L'helguen, S., Le Corre, P., 2000. Nitrogen Uptake by Phytoplankton in a
1039   Shallow Water Tidal Front. Estuarine, Coastal and Shelf Science 51, 349–357.
1040   https://doi.org/10.1006/ecss.2000.0678

1041 Major, Y., Kifle, D., Niedrist, G.H., Sommaruga, R., 2017. An isotopic analysis of the
1042   phytoplankton–zooplankton link in a highly eutrophic tropical reservoir dominated by
1043   cyanobacteria. Journal of Plankton Research 39, 220–231.
1044   https://doi.org/10.1093/plankt/fbx007

1045 Mason, R.P., Reinfelder, J.R., Morel, F.M.M., 1995. Bioaccumulation of mercury and
1046   methylmercury. Water Air Soil Pollut 80, 915–921. https://doi.org/10.1007/BF01189744

1047 Mauchline, J., 1998. The biology of Calanoid copepods. In: Blaxter, J.H.S., Southward, A.J.,
1048   Tyler, P.A.(Eds.), Advances in Marine Biology, 245–292. Academic Press, San Diego,
1049   USA.

1050 Mayot, N., D'Ortenzio, F., Uitz, J., Gentili, B., Ras, J., Vellucci, V., Golbol, M., Antoine, D.,
1051   Claustre, H., 2017. Influence of the Phytoplankton Community Structure on the Spring
1052   and Annual Primary Production in the Northwestern Mediterranean Sea. Journal of
1053   Geophysical Research: Oceans 122, 9918–9936. https://doi.org/10.1002/2016JC012668

1054   Mayzaud, P., Chanut, J., Ackman, R., 1989. Seasonal changes of the biochemical composition

1055   of marine particulate matter with special reference to fatty acids and sterols. Marine

1056   Ecology Progress Series 56, 189–204. https://doi.org/10.3354/meps056189

1057   Montoya, J.P., Carpenter, E.J., Capone, D.G., 2002. Nitrogen fixation and nitrogen isotope

1058   abundances in zooplankton of the oligotrophic North Atlantic. Limnology and

1059   Oceanography 47, 1617–1628. https://doi.org/10.4319/lo.2002.47.6.1617

1060   Morris, M.J., Hopkins, T.L., 1983. Biochemical composition of crustacean zooplankton from

1061   the eastern Gulf of Mexico. Journal of Experimental Marine Biology and Ecology 69, 1–

1062   19.

1063   Motwani, N.H., Gorokhova, E., 2013. Mesozooplankton Grazing on Picocyanobacteria in the

1064   Baltic Sea as Inferred from Molecular Diet Analysis. PLOS ONE 8, e79230.

1065   https://doi.org/10.1371/journal.pone.0079230

1066   Onodera, T., Kanaya, G., Hatamoto, M., Kohzu, A., Iguchi, A., Takimoto, Y., Yamaguchi, T.,

1067   Mizuochi, M., Syutsubo, K., 2018. Evaluation of trophic transfer in the microbial food

1068   web during sludge degradation based on 13C and 15N natural abundance. Water

1069   Research 146, 30–36. https://doi.org/10.1016/j.watres.2018.09.016

1070   Ostrom, P. H., Fry, B., 1993. Sources and cycling of organic matter within modern and

1071   prehistoric food webs. Organic geochemistry, 785-798. Springer, Boston, MA.

1072   Pantoja, S., Repeta, D.J., Sachs, J.P., Sigman, D.M., 2002. Stable isotope constraints on the

1073   nitrogen cycle of the Mediterranean Sea water column. Deep Sea Research Part I:

1074   Oceanographic Research Papers 49, 1609–1621. https://doi.org/10.1016/S0967-

1075   0637(02)00066-3

1076   Parnell, A.C., Phillips, D.L., Bearhop, S., Semmens, B.X., Ward, E.J., Moore, J.W., Jackson,

1077   A.L., Grey, J., Kelly, D.J., Inger, R., 2013. Bayesian stable isotope mixing models.

1078   Environmetrics 24, 387–399. https://doi.org/10.1002/env.2221

1079   Peterson, B.J., Howarth, R.W., Garritt, R.H., 1985. Multiple stable isotopes used to trace the

1080   flow of organic matter in estuarine food webs. Science 227, 1361–1363.

1081   https://doi.org/10.1126/science.227.4692.1361

1082   Phillips, D.L., Inger, R., Bearhop, S., Jackson, A.L., Moore, J.W., Parnell, A.C., Semmens,

1083   B.X., Ward, E.J., 2014. Best practices for use of stable isotope mixing models in food-

1084   web studies. Canadian Journal of Zoology 92, 823–835. https://doi.org/10.1139/cjz-2014-

1085   0127

1086 Pinnegar, J.K., Polunin, N.V.C., 1999. Differential fractionation of δ13C and δ15N among

1087   fish tissues: implications for the study of trophic interactions. Functional Ecology 13,

1088   225–231. https://doi.org/10.1046/j.1365-2435.1999.00301.x

1089 Post, D.M., 2002. Using Stable Isotopes to Estimate Trophic Position: Models, Methods, and

1090   Assumptions. Ecology 83, 703–718. https://doi.org/10.1890/0012-

1091   9658(2002)083[0703:USITET]2.0.CO;2

1092 Postel, L., Fock, H., Hagen, W., 2000. 4 - Biomass and abundance, In: Harris, R., Wiebe, P.,

1093   Lenz, J., Skjoldal, H.R., Huntley, M. (Eds.), ICES Zooplankton Methodology Manual.

1094   Academic Press, London, pp. 83–192. https://doi.org/10.1016/B978-012327645-2/50005-

1095   0

1096 Raimbault, P., Diaz, F., Pouvesle, W., Boudjellal, B., 1999. Simultaneous determination of

1097   particulate organic carbon, nitrogen and phosphorus collected on filters, using a semi-

1098   automatic wet-oxidation method. Marine Ecology Progress Series 180, 289.

1099 Raimbault, P., Garcia, N., Cerutti, F., 2008. Distribution of inorganic and organic nutrients in

1100   the South Pacific Ocean; evidence for long-term accumulation of organic matter in

1101   nitrogen-depleted waters. Biogeosciences 5, 281–298. https://doi.org/10.5194/bg-5-281-

1102   2008

1103 Rau, G., Teyssie, J., Rassoulzadegan, F., Fowler, S., 1990. C-13/C-12 and N-15/N-14

1104   variations among size-fractionated marine particles - implications for their origin and

1105   trophic relationships. Marine Ecology Progress Series 59(1/2), 33–38.

1106 Ríos, A.F., Fraga, F., Pérez, F.F., Figueiras, F.G., 1998. Chemical composition of

1107   phytoplankton and Particulate Organic Matter in the Ría de Vigo (NW Spain). Scientia

1108   Marina 62 (3), 257–271 https://doi.org/10.3989/scimar.1998.62n3257

1109 Rolff, C., 2000. Seasonal variation in δ13C and δ15N of size-fractionated plankton at a

1110   coastal station in the northern Baltic proper. Marine Ecology Progress Series 203, 47–65.

1111   https://doi.org/10.3354/meps203047

1112 Ryther, J.H., 1969. Photosynthesis and Fish Production in the Sea. Science 166, 72–76.

1113   https://doi.org/10.1126/science.166.3901.72

1114 Schartup, A.T., Qureshi, A., Dassuncao, C., Thackray, C.P., Harding, G., Sunderland, E.M.,

1115   2018. A Model for Methylmercury Uptake and Trophic Transfer by Marine Plankton.

1116   Environmental Science & Technology 52, 654–662.

1117   https://doi.org/10.1021/acs.est.7b03821

Sommer, F., Stibor, H., Sommer, U., Velimirov, B., 2000. Grazing by mesozooplankton from Kiel Bight, Baltic Sea, on different sized algae and natural seston size fractions. Marine Ecology Progress Series 199, 43–53. https://doi.org/10.3354/meps199043

Sommer, U., Stibor, H., Katechakis, A., Sommer, F., Hansen, T., 2002. Pelagic food web configurations at different levels of nutrient richness and their implications for the ratio fish production:primary production, in: Vadstein, O., Olsen, Y. (Eds.), Sustainable Increase of Marine Harvesting: Fundamental Mechanisms and New Concepts. Springer Netherlands, Dordrecht, pp. 11–20. https://doi.org/10.1007/978-94-017-3190-4_2

Søreide, J.E., Hop, H., Carroll, M.L., Falk-Petersen, S., Hegseth, E.N., 2006. Seasonal food web structures and sympagic–pelagic coupling in the European Arctic revealed by stable isotopes and a two-source food web model. Progress in Oceanography 71, 59–87. https://doi.org/10.1016/j.pocean.2006.06.001

Tamelander, T., Kivimäe, C., Bellerby, R.G.J., Renaud, P.E., Kristiansen, S., 2009. Base-line variations in stable isotope values in an Arctic marine ecosystem: effects of carbon and nitrogen uptake by phytoplankton. Hydrobiologia 630, 63–73. https://doi.org/10.1007/s10750-009-9780-2

Tao, Y., Yu, J., Liu, X., Xue, B., Wang, S., 2018. Factors affecting annual occurrence, bioaccumulation, and biomagnification of polycyclic aromatic hydrocarbons in plankton food webs of subtropical eutrophic lakes. Water Research 132, 1–11. https://doi.org/10.1016/j.watres.2017.12.053

Tedetti, M., Tronczynski, J., 2019. HIPPOCAMPE cruise, RV Antea. https://doi.org/10.17600/18000900

Tedetti, M., Tronczynski, J., Carlotti, J.F., Pagano, M., Ben Ismail, S., Sammari, C., Bel Hassen, M., Desboeufs, K., Poindron, C., Chifflet, S., Bellaaj Zouari, A., Abdennadher, M., Amri, S., Bănaru, D., Ben Abdallah, L., Bhairy, N., Boudriga, I., Bourin, A., Brach-Papa, C., Briant, N., Cabrol, L., Chevalier, C., Chouba, L., Coudray, S., Daly Yahia, M. N., de Garidel Thoron, T., Dufour, A., Dutay, J-C., Espinasse, B., Fierro-González, P., Fornier, M., Garcia, N., Giner, F., Guigue, C., Guilloux, L., Hamza, A., Heimbürger-Boavida, L-E., Jacquet, S., Knoery, J., Lajnef, R., Makhlouf Belkahia, N., Malengros, D., Martinot, P.L., Bosse, A., Mazur, J-C., Meddeb, M., Misson, B., Pringault, O., Quéméneur, M., Radakovitch, O., Raimbault, P., Ravel, R., Rossi, R., Rwawi, C., Sakka Hlaili, A., Tesán-Onrubia, J.A., Thomas, B., Thyssen, M., Zaaboub, N., Garnier, C., 2023. Contamination of planktonic food webs in the Mediterranean Sea: Setting the

1151   frame for the MERITE-HIPPOCAMPE oceanographic cruise (spring 2019). Marine

1152   Pollution Bulletin. In press in this special issue.

1153   Tiano, M., Tronczyński, J., Harmelin-Vivien, M., Tixier, C., Carlotti, F., 2014. PCB

1154   concentrations in plankton size classes, a temporal study in Marseille Bay, Western

1155   Mediterranean Sea. Marine Pollution Bulletin 89, 331–339.

1156   https://doi.org/10.1016/j.marpolbul.2014.09.040

1157   Tiselius, P., Fransson, K., 2016. Daily changes in $\delta15N$ and $\delta13C$ stable isotopes in copepods:

1158   equilibrium dynamics and variations of trophic level in the field. Journal of Plankton

1159   Research 38, 751–761. https://doi.org/10.1093/plankt/fbv048

1160   Trimble, S.M., Baskaran, M., 2005. The role of suspended particulate matter in 234Th

1161   scavenging and 234Th-derived export fluxes of POC in the Canada Basin of the Arctic

1162   Ocean. Marine Chemistry 96, 1–19. https://doi.org/10.1016/j.marchem.2004.10.003

1163   Vander Zanden, M.J.V., Rasmussen, J.B., 2001. Variation in $\delta15N$ and $\delta13C$ trophic

1164   fractionation: Implications for aquatic food web studies. Limnology and Oceanography

1165   46, 2061–2066. https://doi.org/10.4319/lo.2001.46.8.2061

1166   Wainright, S.C., Fry, B., 1994. Seasonal variation of the stable isotopic compositions of

1167   coastal marine plankton from Woods Hole, Massachusetts and Georges Bank. Estuaries

1168   17, 552–560. https://doi.org/10.2307/1352403

1169   Wu, Y., Wang, W.-X., 2011. Accumulation, subcellular distribution and toxicity of inorganic

1170   mercury and methylmercury in marine phytoplankton. Environmental Pollution, Nitrogen

1171   Deposition, Critical Loads and Biodiversity 159, 3097–3105.

1172   https://doi.org/10.1016/j.envpol.2011.04.012

1173   Yang, G., Li, C., Guilini, K., Wang, X., Wang, Y., 2017. Regional patterns of $\delta13C$ and $\delta15N$

1174   stable isotopes of size-fractionated zooplankton in the western tropical North Pacific

1175   Ocean. Deep Sea Research Part I: Oceanographic Research Papers 120, 39–47.

1176   https://doi.org/10.1016/j.dsr.2016.12.007

1177   Yılmaz, A.Z., Besiktepe, S., 2010. Annual variations in biochemical composition of size

1178   fractionated particulate matter and zooplankton abundance and biomass in Mersin Bay,

1179   NE Mediterranean Sea. Journal of Marine Systems 81, 260–271.

1180   https://doi.org/10.1016/j.jmarsys.2010.01.002

1181

Figure captions

1183

Figure 1. Location of the ten sampling stations of the MERITE-HIPPOCAMPE campaign in the Mediterranean Sea (April-Mai 2019).

1186

Figure 2. Boxplot of the concentrations of A) proteins, B) carbohydrates, C) lipids (μg mg^{-1} DW) and D) energy content (E_i) (kJ g^{-1} DW) in the different plankton size-fractions (fractions between 0.7 and 60 μm in green and > 60 μm in orange) for all stations combined. H = Kruskal–Wallis non-parametric test and the associated p-value for the respective biochemical compounds: H = 43.5, p < 0.0001; H = 110.6, p < 0.001; H = 41.8, p < 0.0001 and H = 51.7, p < 0.0001. Mean values with different letters are significantly different (p < 0.05). The mean and median values are represented by a cross and a horizontal line, respectively, and the box length is defined as the interquartile range. The minimum and maximum values are represented by whiskers. Mean values with different post-hoc letters are significantly different (p < 0.05).

1195

Figure 3. Boxplot of the concentrations of A, B) proteins, C, D) carbohydrates, E, F) lipids (μg mg^{-1} DW) and G, H) energy content (E_i) (kJ g^{-1} DW) in the phyto- (fractions between 0.7 and 60 μm – in green) and zooplankton (fractions between 60 and 500 μm – in orange) fractions for each station. H = Kruskal–Wallis non-parametric test and the associated p-value for the respective biochemical compounds for phytoplankton (H = 43.4, p < 0.0001; H = 30.6, p < 0.0001; H = 34.9, p < 0.0001 and H = 42.9, p < 0.0001) and for zooplankton (H = 43.8, p < 0.0001; H = 22.9, p < 0.006; H = 38.8, p < 0.0001 and H = 38.8, p < 0.0001). Stations are grouped by geographical area: St1, St2, St3 and St4 for the Northern coast, St9, St10 and St11 for the offshore area, and St15, St17 and St19 for the Southern coast. The mean and median values were represented by a cross and a horizontal line, respectively, and the box length is defined as the interquartile range. The minimum and maximum values are represented by whiskers. Mean values with different post-hoc letters are significantly different (p < 0.05).

1207

Figure 4. Total amount of energy provided by plankton (E_T in kJ m^{-3}) for each of the size-fractions by station. Stations are grouped by geographical area: St1, St2, St3 and St4 for the Northern coast, St9, St10 and St11 for the offshore area, and St15, St17 and St19 for the Southern coast.

1211

Figure 5. Mean ($\pm$ standard error, SE) stable isotope compositions (δ^{13}C and δ^{15}N values, ‰) in the different plankton size-fractions for all stations combined. Green dots correspond to the phytoplankton size-fractions (from 0.7 to 60 μm), while the orange dots correspond to zooplankton size-fractions (> 60 μm).

1215

Figures 6. Boxplot of the A, B) δ^{13}C and C, D) δ^{15}N values (‰) in the phyto- (fractions between 0.7 and 60 μm – in green) and zooplankton (fractions between 60 and 500 μm – in orange) fractions for each station. Stations are grouped by geographical area: St1, St2, St3 and St4 for the Northern coast, St9, St10 and St11 for the offshore area, and St15, St17 and St19 for the Southern coast. Kruskall-Wallis non-parametric test were performed for A) (H = 25.5, p < 0.05), C) (H = 24.1, p < 0.05) and D) (H = 33.5, p < 0.0001), and one-way

1221 ANOVA test was performed for B) (F = 4.4, p < 0.0001). The mean and median values are represented by a

1222 cross and a horizontal line, respectively, and the box length is defined as the interquartile range. The minimum

1223 and maximum values are represented by whiskers. Mean values with different post-hoc letters are significantly

1224 different (p < 0.05).

1225

1226 **Figure 7.** Boxplot of the trophic levels (TL) of the zooplankton size-fractions (60 to > 2000 µm). The median

1227 value is represented by a horizontal line and the box length is defined as the interquartile range. The minimum

1228 and maximum values are represented by whiskers. One-way ANOVA test (F = 5.17, p = 0.001). Superscript

1229 letters represent Newman-Keuls post-hoc groups and values with the different letters are significantly different

1230 (p < 0.05).

1231

1232 **Figure 8.** Trophic levels (TL) of the zooplankton size-fractions (60 to > 2000 µm) and mean TL weighted by

1233 their biomass (TL$_B$) for each station. Stations are gathered by geographical area: St1, St2, St3 and St4 for the

1234 Northern coast, St9, St10 and St11 for the offshore area, and St15, St17 and St19 for the Southern coast.

1235

1236 **Figure 9.** Relative contributions of 0.7–2.7 µm (pico-), 2.7–20 µm (nano-), and 20–60 µm (microplankton) as

1237 food resources for three zooplankton size-fractions. Arrows indicate the trophic transfer between pico-POM

1238 nano-POM, and micro-POM fractions and zooplankton size fractions: 60–500 µm (in green), 500–2000 µm (in

1239 blue) and > 2000 µm (in orange). Their thickness is proportional to relative contribution in percentage, indicated

1240 close to the corresponding arrow.

1241

1242 **Table 1.** Suspended particulate matter and plankton dry weight (SPM$_{DW}$ and Plankton$_{DW}$, in mg DW L^{-1}) for the

1243 different plankton size-fractions and stations, as well as total chlorophyll *a* concentration (TChl*a*, µg L^{-1}) for the

1244 > 0.7-µm fraction. Kruskal-Wallis test and the associated p-value for SPM$_{DW}$ (H = 23.15, p < 0.0001) and

1245 Plankton$_{DW}$ (H = 28.51, p < 0.0001). Superscript letters represent rank comparison groups and values with

1246 different letters are significantly different (p < 0.05). St = station, SE = standard-error, n = number of samples.
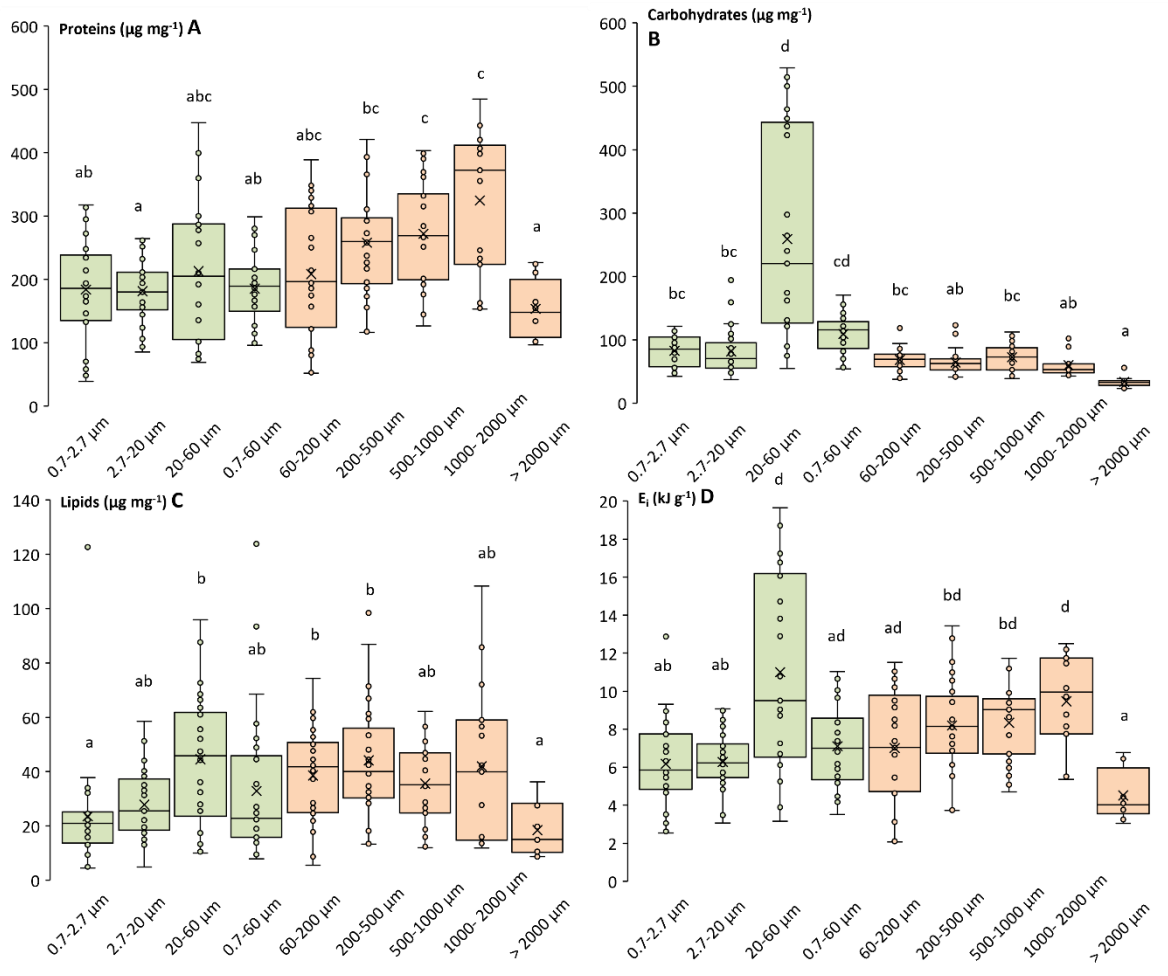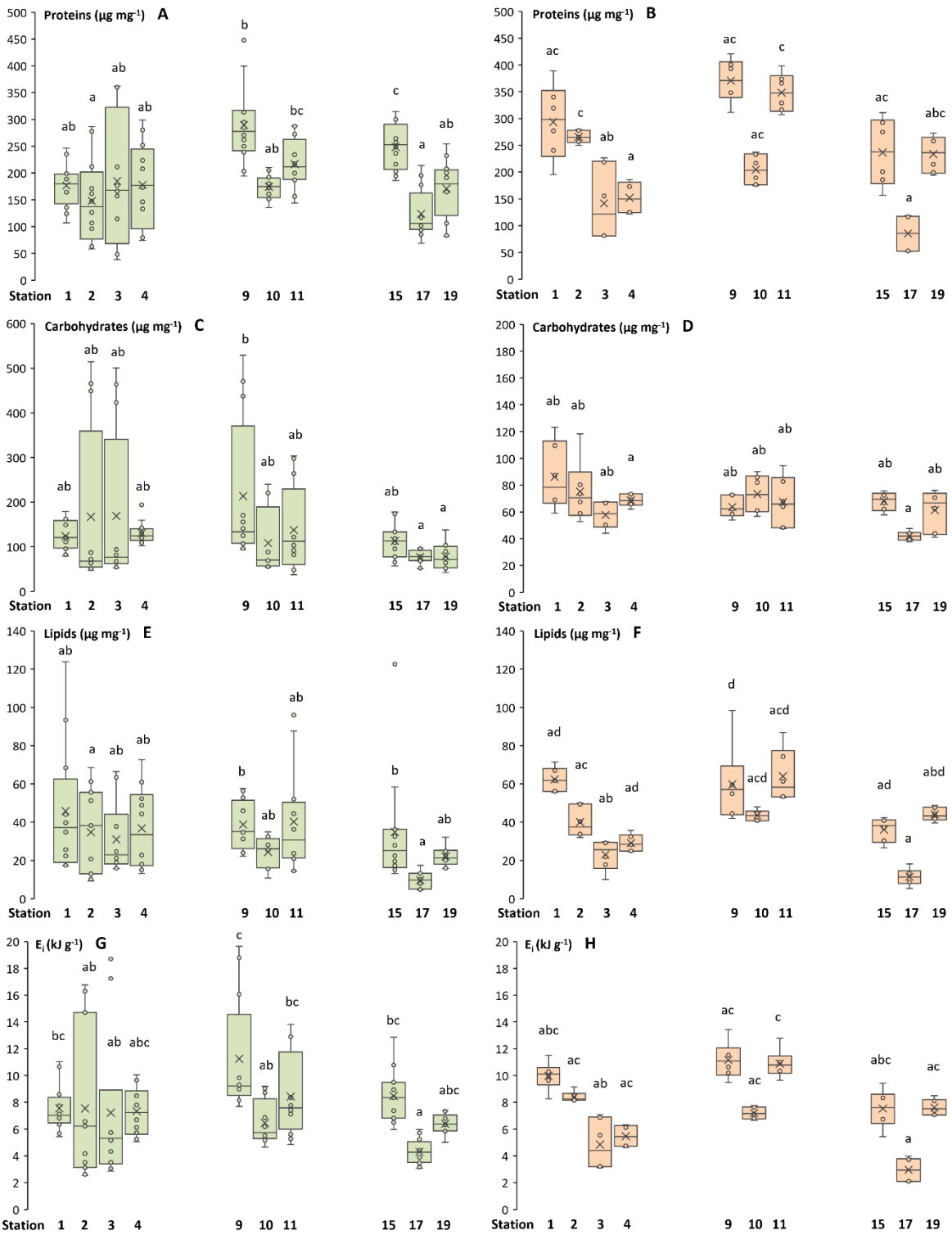
1247

Figures
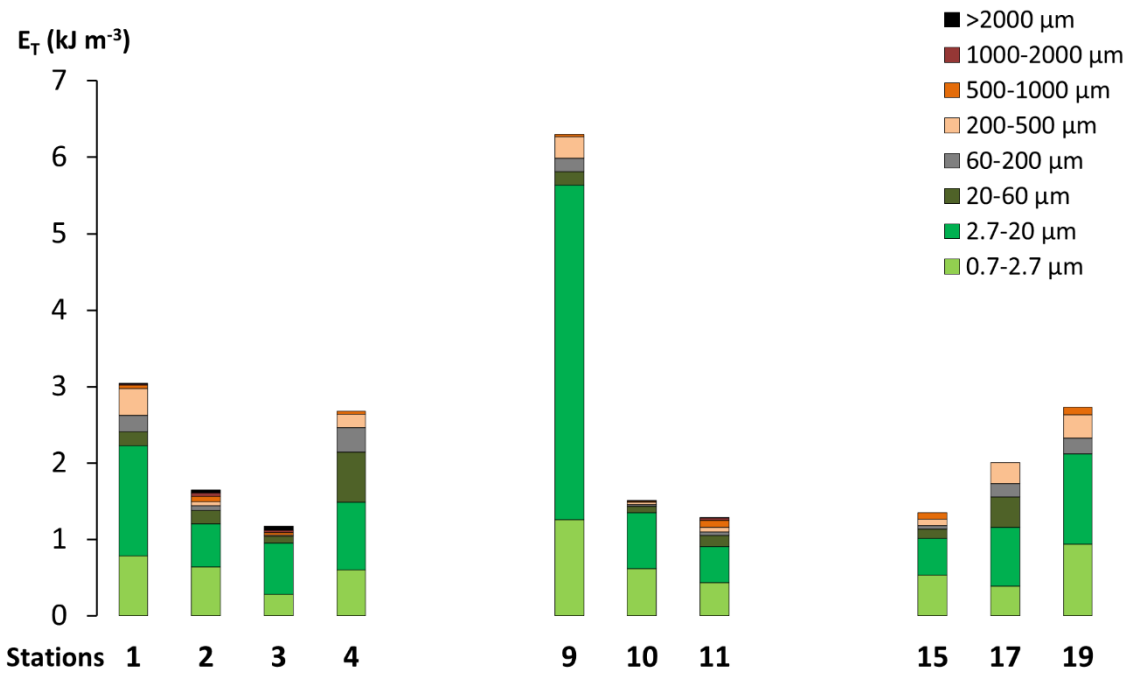
Figure 1

1253

1254
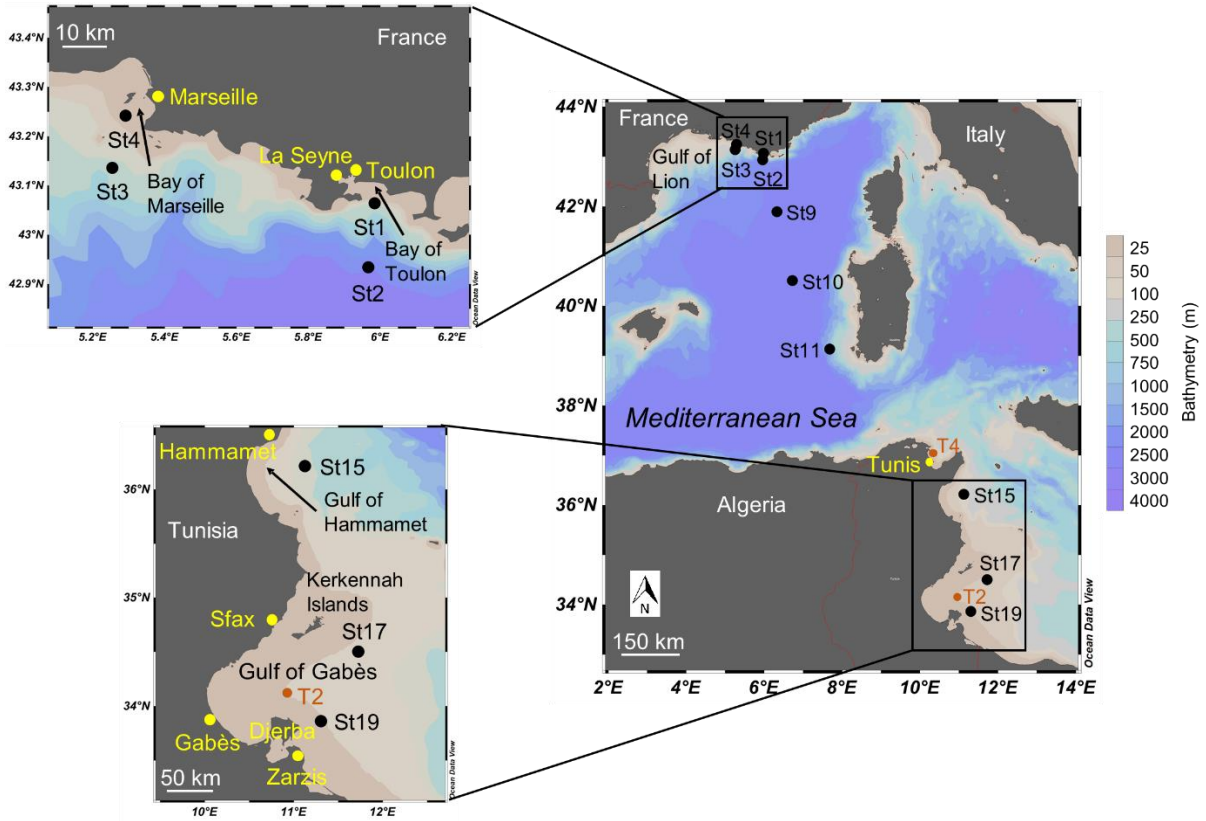
Figure 2

1256

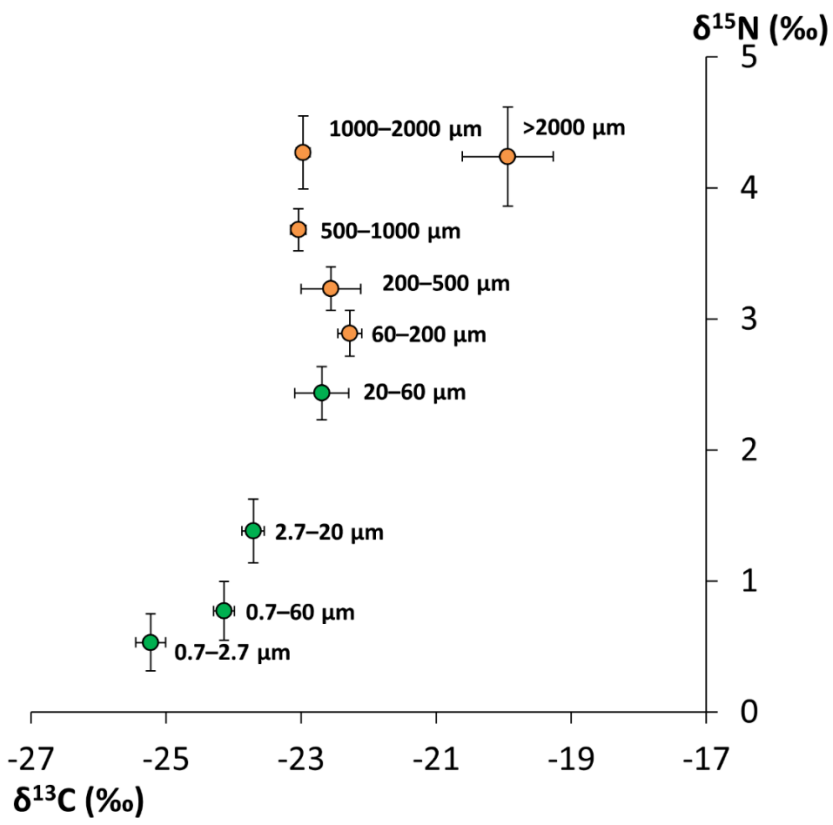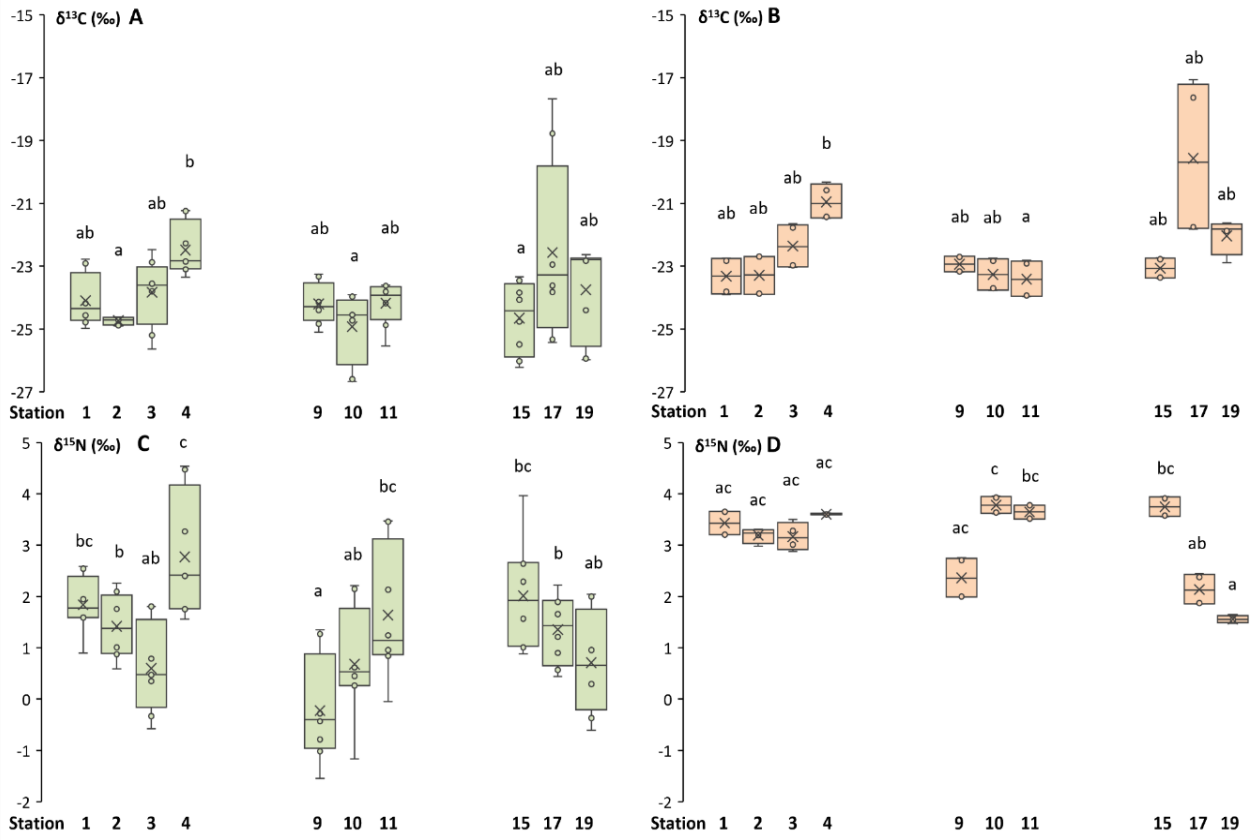1257 **Figure 3**

1258

1259   **Figure 4**

1260

1261

1262 **Figure 5**

1263

1264

Figure 6

1266

1267
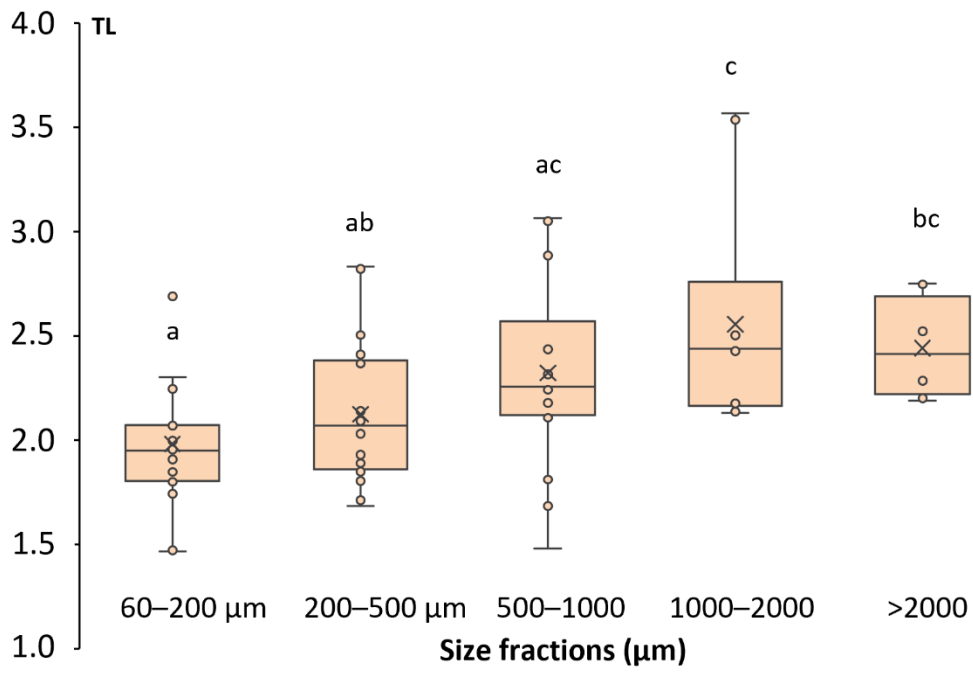
1268

1269 **Figure 7**

1270

1271

1272 **Figure 8**

1273

60-500 µm   **500-2000 µm**   **> 2000 µm**

46%   47%   7%   28%   56% 16%   6%   6%   88%

0.7-2.7 µm   **2.7-20 µm**   **20-60 µm**
PICO   **NANO**   **MICRO**
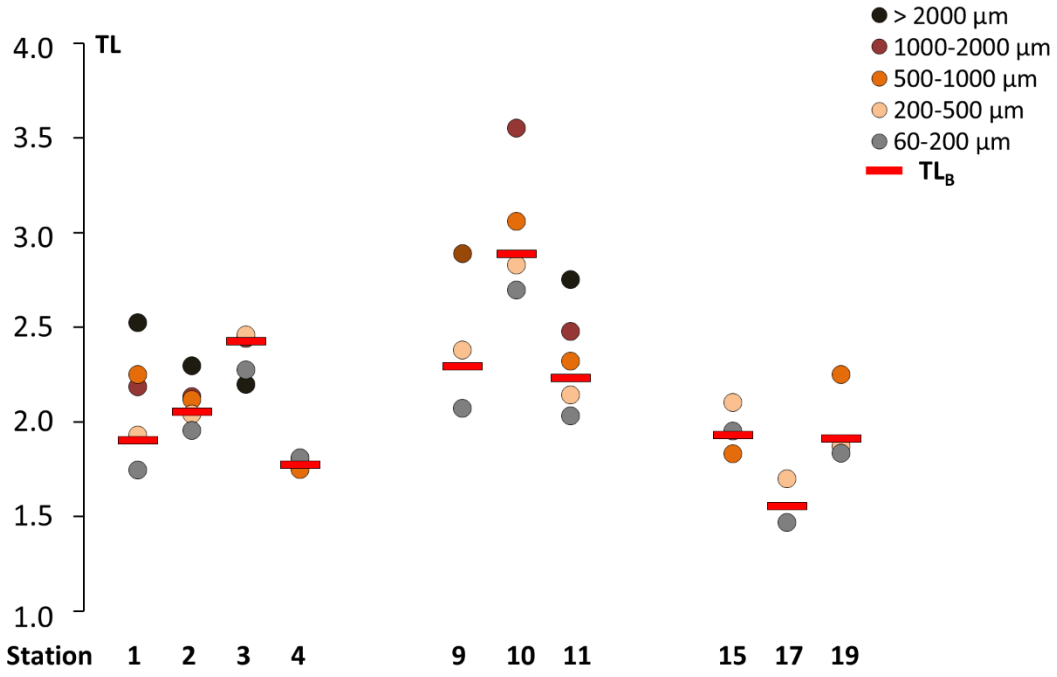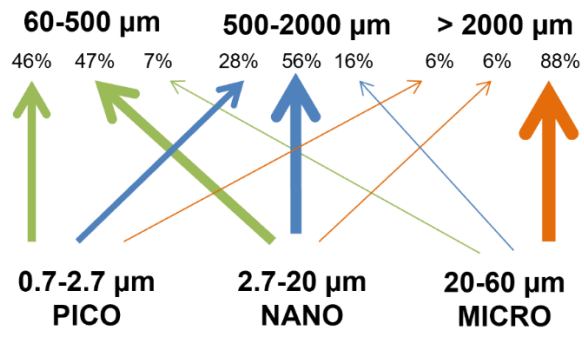
1274

1275   **Figure 9**

1276

1277 **Tables**

1278 **Table 1.**

Stations	St1	St2	St3	St4	St9	St10	St11	St15	St17	St19	n	Mean ± SE			
Size-fractions						SPM_{DW} (mg DW L^{-1})									
0.7–2.7 µm	0.11	0.23	0.09	0.11	0.14	0.12	0.06	0.05	0.07	0.16	10	0.11	±	0.02	[ab]
2.7–20 µm	0.24	0.09	0.12	0.11	0.53	0.13	0.09	0.07	0.23	0.17	10	0.18	±	0.04	[bc]
20–60 µm	0.03	0.01	0.00	0.11	0.01	0.01	0.01	0.01	0.11	0.11	10	0.04	±	0.02	[a]
0.7–60 µm	0.35	0.32	0.21	0.22	0.67	0.25	0.15	0.12	0.29	0.34	10	0.29	±	0.05	[c]
TChl*a* (> 0.7 µm) (µg L^{-1})	0.77	0.38	0.68	0.98	1.54	0.55	0.38	0.67	0.21	1.45	10	0.76	±	0.14	
						$Plankton_{DW}$ (mg DW L^{-1})									
60–200 µm	0.020	0.007	0.002	0.068	0.017	0.003	0.004	0.006	0.083	0.029	10	0.024	±	0.027	[ab]
200–500 µm	0.037	0.007	0.002	0.028	0.023	0.004	0.005	0.010	0.072	0.038	10	0.023	±	0.021	[ab]
500–1000 µm	0.005	0.007	0.004	0.007	0.004	0.002	0.009	0.009	0.002	0.011	10	0.006	±	0.003	[b]
1000–2000 µm	0.002	0.005	0.007	0.002	0.0002	0.001	0.002	0.001		0.0000	10	0.002	±	0.002	[a]
> 2000 µm	0.0004	0.005	0.013			0.0001	0.0004	0.001		0.0002	10	0.003	±	0.005	[a]
Sum 60–>2000 µm	0.064	0.031	0.028	0.105	0.044	0.011	0.020	0.026	0.157	0.078	50	0.057	±	0.019	

1279